Density Functional Theory Description of II-VI Compounds

Master Thesis

Jean-René Moret

Project director: Prof. A. Baldereschi

January 23, 2009

ÉCOLE POLYTECHNIQUE
FÉDÉRALE DE LAUSANNE

Contents

1 Introduction **2**

2 Theoretical background **2**
2.1 Born-Oppenheimer approximation . . . 2
2.2 DFT, Kohn-Sham ansatz and exchange-correlation functionals . . . 3
2.2.1 Local density approximation . . . 3
2.2.2 Generalised gradient approximations . . . 4
2.2.3 Exact exchange and hybrid functionals . . . 4
2.2.4 Density functional approximation with Hubbard term . . . 6
2.3 Pseudopotentials . . . 6
2.3.1 Unscreening and core corrections . . . 7
2.4 Structures . . . 8
2.5 *p*-*d* mixing . . . 9

3 Methods **10**
3.1 Supercell approach . . . 10
3.2 Code . . . 10
3.3 Ionic structure relaxation . . . 10
3.4 Murnaghan's equation of state . . . 11
3.5 Band structures and projected densities of states . . . 11

4 Generating and testing pseudopotentials **12**
4.1 Magnesium . . . 12
4.2 Zinc . . . 12
4.3 Oxygen and sulphur . . . 14
4.4 Selenium . . . 14
4.5 Cobalt . . . 15

5 Magnesium Chalcogenides **18**
5.1 Structures and relative stability . . . 18
5.2 Electronic structure . . . 20

6 Zinc Chalcogenides **25**
6.1 Structural properties using PBE . . . 25
6.2 Electronic properties using GGA and hybrid functionals . . . 25
6.2.1 Analysis and comments . . . 25
6.2.2 Proposed solutions . . . 31
6.3 Modified pseudopotential approach and its effects . . . 32
6.3.1 Principle and method . . . 32
6.3.2 Effects on structure . . . 32
6.3.3 Effects on electronic structure . . . 32
6.3.4 Discussion . . . 36

7 Applications **36**
7.1 $ZnO_{1-x}S_x$ . . . 37
7.2 Cobalt doped ZnO . . . 38

8 Conclusion **42**

9 Acknowledgements **42**

List of figures **43**

List of tables **43**

References **44**

1 Introduction

II-VI semiconductors are a subject of great interest, from both theoretical and experimental point of view. This interest originates from several known, developing or proposed applications. As wide-gap semiconductors, these compounds find applications in blue and green light emitting devices [20]. Zinc oxide, being a transparent material and subject to strong n-type doping, is a material of choice for transparent electrodes (*e.g* [32]); it is also a well know piezoelectric material [15]. It has also been shown recently that ZnO doped with cobalt and other transitions metal exhibits –under certain conditions– dilute magnetic semiconductor (DMS) behaviour with high Curie temperature [28, 57, 58]. The explanation and the conditions for this behaviour are still under a debate ([31, 62] and references therein).

Ternary and quaternary II-VI compounds are also a field of interest, because they may give access to lattice-matching with other semiconductors and controllable gap, with potential applications in opto-electronics and quantum wells.

In these fields of research, density functional theory (DFT) has the potential to become a major tool for the prediction of properties of novel materials and interpretation of experimental results(*e.g.* [31, 47, 62]). However, a fully consistent *ab-initio* description of those materials has not been achieved up to date ; existing methods either rely on (sometime massive) case-specific *ad-hoc* corrections or fail on predicting certain key properties, *i.e.* band gaps are severely underestimated and d-bands are too shallow in regard of the valence band maximum, as compared to photo emission data.

In this work, we will study the description of binary II-VI compounds by DFT using generalized gradient approximation (section 2.2.2) and more accurate hybrid exchange-correlation (XC) functionals (section 2.2.3), which improve band gaps and partly correct the self-interaction problem of DFT. However, hybrid functionals fail to correct the position of d-bands in zinc compounds and to reproduce the experimental gap in ZnO. We show that these shortcoming are directly related, so that we propose a semi-empirical way to correct the position of d-bands and to obtain correct key electronic properties. The successes and shortcomings of this method will be assessed. Preliminary applications in more complex systems, namely cobalt doped ZnO and the ternary compound $ZnO_{1-x}S_x$, will be presented in order to test its applicability, which is only partial.

2 Theoretical background

2.1 Born-Oppenheimer approximation

Our study of II-VI semiconductors will rely on several approximations ; the first and most widespread one is the Born-Oppenheimer [7] approximation: knowing that nuclei are much heavier than electrons, one considers that their motion takes place on a time scale long enough for the electrons to readjust exactly whenever the nuclei move. Namely, this means

that the electronic structure depends only on the nuclei's positions and not on their speeds or momenta.

2.2 DFT, Kohn-Sham ansatz and exchange-correlation functionals

In order to treat the degrees of freedom of the system, we are using the Density Functional Theory, based on the two theorems by Hohenberg and Kohn [23], which show that all properties of a system can be deduced from the ground state electronic density only, and that this density can be found by minimising the expectation value of the Hamiltonian as a functional of the density.

We will be working within the Kohn-Sham [30] *ansatz*, which consists of the replacement of the original many-electron problem by a problem of fictious non-interacting (pseudo)electrons in a self-consistent, density-dependant potential (Kohn-Sham (KS) potential). The non-interacting problem is devised as to reproduce the density of the interacting electrons. In this *ansatz*, the kinetic energy is obtained directly from the non-interacting wavefunctions, while other energetic terms are computed from the density. The Kohn-Sham potential (eq. (1)) is determined by the ionic coulomb potential, by a Hartree term which describes electron-electron classical coulomb interaction, and by a so-called exchange-correlation term, which describes quantum corrections to electron-electron interaction, effects of correlation, and corrections to the kinetic energy between the true interacting electrons and the Kohn-Sham non-interacting electrons.(One illustration of this last type of correction is to think that when electrons correlate, they may adopt wavefunctions which are kinetically less optimal than the non-interacting one, but allow greater gain in correlation and/or exchange energy)

$$V_{KS}^{\sigma}([n],\vec{r}) = V_{ext}(\vec{r}) + V_{Hartree}([n],\vec{r}) + V_{XC}^{\sigma}([n],\vec{r}) \tag{1}$$

With $V_{KS}^{\sigma}([n],\vec{r})$ the effective Kohn-Sham potential (at position $\vec{r}$, with a functional dependance on the density n), $V_{ext}(\vec{r})$ the ionic coulomb potential, $V_{XC}^{\sigma}([n],\vec{r})$ the exchange-correlation term and σ the spin index. The non-interacting pseudo-electrons are then described by the Hamiltonian (2)

$$H_{KS}^{\sigma}([n],\vec{r}) = -\frac{1}{2}\nabla^2 + V_{KS}^{\sigma}([n],\vec{r}) \tag{2}$$

Unfortunately, the effect of exchange and correlation is not known exactly, therefore our second approximation resides in the choice of an exchange-correlation (XC) functional ; we present some of the main families of XC functionals in the following subsections.

All the potential terms are dependant on the electronic density, which lead to a "self consistent-field" (SCF) calculation: the density is computed from the KS wavefunctions ; this density leads to calculation of a new KS potential, which is in turn used to calculate new wavefunctions, and so on until the density and potential vary little enough from one iteration to the next one.

2.2.1 Local density approximation

The first proposed XC functionals were based on the local density approximation (LDA), as proposed by Kohn and Sham [30]. Its principle is to take the exchange and correlation energy density at each point to be that of an homogeneous gas of electrons of the same density.(eq. (3))

$$E_{XC}^{LDA}[n] = \int \mathrm{d}^3 r n(\vec{r}) \epsilon_{XC}^{hom}(n(\vec{r}) \tag{3}$$

With $E_{XC}^{LDA}[n]$ the LDA exchange correlation functional (in the spin unpolarized case), $n(\vec{r})$ the local density and ϵ_{XC}^{hom} the exchange-correlation energy density of a non interacting electron gas, as a function of the electronic density.

The more inhomogenous the density is, the less accurate this simple approximation should become, however error cancellation makes it perform acceptably in many inhomogenous cases. It generally yields acceptable results for structural quantities, and was the backbone of DFT calculation for more than a decade.

2.2.2 Generalised gradient approximations

The next milestone in the domain of XC functionals was the advent of generalised gradient approximation based XC functionals (GGAs). These functionals do not express the XC energy density only as a function of the local density, but take into account it's gradient. They have shown greater accuracy than LDA in many systems, especially in computing energetic values [48]. Our reference GGA for this work will be the one devised by Perdew, Burke and Ernzerhof (PBE, see [48]), which is also the basis of the PBE0 hybrid functional.

2.2.3 Exact exchange and hybrid functionals

Hybrid functionals are a class of XC functional which include partially exact (Fock) exchange, along with some GGA (or similar) exchange and correlation.

One first reason to take exact exchange into account is that the true effect of exchange is non-local, whereas GGAs are only semilocal. Another reason is because of the self-interaction problem of the Hartree term. It is usual to write the Hartree and Fock terms as in equation (4) and (5), were in both case the $i = j$ "self-interaction" is included. This term is spurious, but cancels out when one include both Hartree and Fock energy.

$$E_{Hartree} = \frac{1}{2} \sum_{i,j,\sigma_i,\sigma_j} \int d\mathbf{r} d\mathbf{r}' \psi_i^{\sigma_i *}(\mathbf{r}) \psi_j^{\sigma_j *}(\mathbf{r}') \frac{1}{|\mathbf{r} - \mathbf{r}'|} \psi_i^{\sigma_i}(\mathbf{r}) \psi_j^{\sigma_j}(\mathbf{r}') \tag{4}$$

$$E_{Fock} = -\frac{1}{2} \sum_{i,j,\sigma} \int d\mathbf{r} d\mathbf{r}' \psi_i^{\sigma *}(\mathbf{r}) \psi_j^{\sigma *}(\mathbf{r}') \frac{1}{|\mathbf{r} - \mathbf{r}'|} \psi_j^{\sigma}(\mathbf{r}) \psi_i^{\sigma}(\mathbf{r}') \tag{5}$$

With $\psi_{i,j}^{\sigma}$ the wavefunction of one electron of spin σ, the sum over i, j running over all possible pair of electron and the integral over $\mathbf{r}$ and $\mathbf{r}'$ running over the whole space.

However, in GGA DFT the Hartree term is included but the Fock term is not included in the form of (5). Instead, the cancellation is approximately done through the XC functional, but part of the self-interaction remains. The self-interaction term is more important for very localised states; this is one reason why d and s or p states are usually not simultaneously well described with GGAs.[1]

A third rationale is that the true exchange functional is believed (according to [38]) to have discontinuities at filled shells, which are crucial for calculation of gaps between filled and empty shells, and occur automatically in an orbital-dependent formulation.

An obvious way to use exact exchange in a Kohn-Sham approach would be to use (5) as the exchange part of the XC functional, and only add a correction to account for correlation effects. In fact this approach was already proposed in the seminal paper by Kohn and Sham [30]. The denomination "exact exchange" may lead to think that this procedure is better than any approximation for exchange, but it is indeed not, for two

[1] One can also correct the self-interaction term more directly through the use of self-interaction corrected (SIC) pseudopotentials or functionals; see Ref. [49]

related reasons. First (5) applied to Kohn-Sham states is the exact exchange *of the non-interacting system*, whereas XC functionals are supposed to mimic the energetic effects of exchange and correlation on an *interacting* gas of electron with the same density as the non-interacting system. Secondly, the name "exchange and correlation" is a bit misleading, as this term also includes changes in kinetic energy due to interactions between electrons. Thus, exact exchange is not bound to be the best description of exchange effects.

A correct theoretical basis to describe the effects of interactions is the so called *adiabatic connection*, which comes from a generalised force theorem (Eq. (6)) applicable to the continuous variation of any parameter (*i.e.* λ) in the Hamiltonian ($\hat{H}$).

$$\frac{\partial E}{\partial \lambda} = \langle \psi_\lambda | \frac{\partial \hat{H}}{\partial \lambda} | \psi_\lambda \rangle + \cancel{\langle \frac{\partial \psi_\lambda}{\partial \lambda} | \hat{H} | \psi_\lambda \rangle} + \cancel{\langle \psi_\lambda | \hat{H} | \frac{\partial \psi_\lambda}{\partial \lambda} \rangle} \tag{6}$$

With ψ_λ the ground state wave function at a given λ, and E the energy. The two last term are equal to 0 as, ψ_λ being the ground state wavefunction, the energy is extremal in regard to any possible variation of this wavefunction.
An integral formulation allows to find a finite energy difference between any two states inked by a continuous variation of the Hamiltonian:

$$\Delta E = \int_{\lambda_1}^{\lambda_2} d\lambda \frac{\partial E}{\partial \lambda} = \int_{\lambda_1}^{\lambda_2} d\lambda \langle \psi_\lambda | \frac{\partial \hat{H}}{\partial \lambda} | \psi_\lambda \rangle \tag{7}$$

This theorem allows "connect" the non-interacting Kohn-Sham system to the true interacting system by continuously "turning on" electron-electron interaction: following Becke [3], if one scales the electron-electron interaction by $e^2 \rightarrow e^2\lambda$, integrating on λ from 0 to 1 allows to find the correct Kohn-Sham exchange and correlation energy (eq. (8)).

$$E_{XC} = \int_0^1 U_{XC}^\lambda d\lambda \tag{8}$$

(With U_{XC}^λ the potential part of exchange and correlation energy at given λ). By the generalised force theorem, this integration includes kinetic energy even though only the potential energy is integrated. U_{XC}^λ is not known in general, but this expression gives a rationale for hybrid functionals: at $\lambda = 0$, U_{XC} is nothing else than the Kohn-Sham exact exchange energy; assuming its variation with λ is somewhat smooth, E_{XC} should include some features from exact exchange. On the other hand, one assumes the $\lambda = 1$ end of the integral should be better described by a local or semilocal XC functional (be it GGA, LDA or another relative; the generic term "Density functional approximation"(DFA) will be used), as they are designed to describe interacting electron gases. Thus, E_{XC} may be described as some combination of exact exchange and a conventional XC functional, i.e :

$$E_{XC}^{hyb} = U_{XC,DFA} + \alpha(E_X - U_{X,DFA}) \tag{9}$$

The value of the α parameter depends on further assumptions on the form of U_{XC}^λ. Perdew, Burke and Ernzerhof [9] proposed a model for U_{XC}^λ [2] which depends on an integer parameter n:

$$U_{XC}^\lambda(n) = U_{XC,DFA}^\lambda + (E_X - U_{X,DFA})(1-\lambda)^{(n-1)} \tag{10}$$

This model indeed reduces to exact exchange at $\lambda = 0$ and to DFA at $\lambda = 1$. Upon integration, this yields

$$E_{XC}^{hyb} = U_{XC,DFA} + \frac{1}{n}(E_X - U_{X,DFA}) \tag{11}$$

[2]Following Becke [3], we use U to denote potential energies and E to denote total energies (including corrections to kinetic energy when relevant). Such a distinction is not made in Ref. [9].

For reasons which we will not present here, they proposed that for most systems a value of $n = 4$ should be appropriate, leading to an α value of 0.25. Combination of this approach with the PBE [48] GGA leads to the so-called PBE0 XC functional, which we will use in this work. However there is no guarantee that $\alpha = 0.25$ is the best choice for all systems, and thus the dependancy of band gaps and d-band positions on α will be studied.

2.2.4 Density functional approximation with Hubbard term

An other approach to correct known shortcomings of DFT is the addition of a Hubbard-like [24] term U to a conventional XC functional, leading to density functional approximation + U (DFA + U, which is often named LDA + U , even when LDA is not the XC functional used). The U term is orbital dependant and usually acts on highly localised atomic-like orbitals, shifting them in order to correct for know errors, *e.g.* those which originate from the self-interaction error.

The U parameter can either be calculated, *e.g.* as in the original publication by Anisimov *et. al.* [1], or adjusted as a semi-empirical parameter.

We do not use DFA + U in this work and thus do not describe it in detail. It is however mentioned, because it is a method often used for zinc compounds, with goal somewhat similar to those for which we modify our pseudopotentials.

2.3 Pseudopotentials

Most atoms – especially the heavier ones – have core electrons which do not participate in chemical bonding and whose wavefunctions are not considerably affected by the environment. Thus, it is common to replace the core electrons and the nuclei by some pseudopotentials (PPs), which will be our third main approximation. These are designed so that beyond a certain "core radius", the valence electrons' wavefunction should be the same as it would within the all-electron atom. This approximation leads to two great gains in terms of computational time: first, it reduces drastically the number of electrons to be simulated; secondly, it reduces the number of plane waves (PWs) basis functions needed for an accurate description of the outer orbitals. These orbitals oscillate on a short space scale close to the nucleus in order to ensure orthogonality with inner shell wave functions. Using a pseudopotential allows to get rid of those oscillations and to have a quite smooth wavefunction inside the core, thus reducing the number of plane waves to be used and sparing computer time.

Several kind of pseudopotentials can be used ; the implementation of hybrid DFT that we use requires the use of norm-conserving [21] pseudopotentials, which are designed so that the normalisation of wavefunctions inside the core region is correct, at some cost in smoothness.

Unlike the Coulomb potential in an all-electron calculation, the pseudopotential inside the core radius is orbital dependent, which means that it is divided in several parts (or channels), one for each angular momentum taken into account (4 in our case; even though no occupied f orbital occur in the elements we consider, f component can be needed to describe bulk orbitals). One channel is chosen as the local part of the PP, while nonlocal corrections are used for the other channels. All nonlocal components vanish outside the core radius.

$$V^l = V_{local} + V^l_{nonlocal} \tag{12}$$

With V^l the potential applicable for angular momentum l, V_{local} the local part of the PP, and $V^l_{nonlocal}$ the non-local correction for l. The pseudopotential production is functional-dependent: the PP is designed to reproduce the all-electron atom *obtained with a certain*

XC functional, when used in a calculation with *that same* functional. However, due to the non-local nature of exact-exchange, generating pseudopotentials for hybrid functionals is a complicated procedure, beyond the reach of this work, thus we will use PBE generated PP for hybrid calculations as well. The limitations of this procedure will be discussed.

2.3.1 Unscreening and core corrections

In the procedure to generate pseudopotentials, one defines a pseudo wavefunction (see Figure 6 for an exemple of pseudo and all-electron wavefunctions) with desired properties, then one inverts the Schrödinger equation to find a potential which leads to this wavefunction. This potential (V^l) also includes the effect of other valence electrons, one then has to "unscreen" this potential in order to get an "ionic" pseudopotential (V^l_{ion}), which includes only the effect of the nucleus and of core electrons.

The simplest way to do this is to substract the Hartree ($V_{hartree}\left(\rho^v\left(\vec{r}\right)\right)$) and exchange-correlation ($V_{XC}\left(\rho^v\left(\vec{r}\right)\right)$) potential due to the valence electron density ρ^v:

$$V^l_{ion}(\vec{r}) = V^l(\vec{r}) - V_{hartree}\left(\rho^v\left(\vec{r}\right)\right) - V_{XC}\left(\rho^v\left(\vec{r}\right)\right) \tag{13}$$

This procedure would be exact if V_{XC} were linear with respect the density, but it is not, which can lead to strong transferability problems. The solution proposed by Louie, Froyen and Cohen (non-linear core correction, NLCC) [34] is to store the core density (or a part of it) as ρ^c and define the ionic PP[3] as:

$$V^l_{ion}(\vec{r}) = V^l(\vec{r}) - V_{ee}\left(\rho^v\left(\vec{r}\right)\right) - V_{XC}\left(\rho^v\left(\vec{r}\right) + \rho^c\left(\vec{r}\right)\right) \tag{14}$$

Then, the XC potential in the production calculation must include both ρ^v and ρ^c. In order to show the advantage of this correction, one can express the difference of potential between the two procedure ($\Delta(\vec{r})$).

$$\Delta(\vec{r}) = \left[-V_{XC}\left(\rho^{v_{ae}}\left(\vec{r}\right) + \rho^c\left(\vec{r}\right)\right) + V_{XC}\left(\rho^{v_{prod}}\left(\vec{r}\right) + \rho^c\left(\vec{r}\right)\right)\right] + \left[V_{XC}\left(\rho^{v_{ae}}\left(\vec{r}\right)\right) - V_{XC}\left(\rho^{v_{prod}}\left(\vec{r}\right)\right)\right] \tag{15}$$

($\rho^{v_{ae}}$: valence density in the all-electron atomic calculation; $\rho^{v_{prod}}$: valence density in the production PP calculation)

Assuming $\rho^{v_{ae}}\left(\vec{r}\right) - \rho^{v_{prod}}\left(\vec{r}\right) = \Delta_{\rho^v}\left(\vec{r}\right)$ and $\rho^c\left(\vec{r}\right)$ are both small –an assumption which is not relevant in the system which need NLCC the most and thus is made here for illustration purposes only– one can rewrite this difference using partial derivatives.

$$\Delta(\vec{r}) = -\Delta_{\rho^v}\left(\vec{r}\right)\frac{\partial V_{XC}}{\partial \rho}\Big|_{(\rho^v+\rho^c)(\vec{r})} + \Delta_{\rho^v}\left(\vec{r}\right)\frac{\partial V_{XC}}{\partial \rho}\Big|_{\rho^v(\vec{r})} \tag{16}$$

$$= -\Delta_{\rho^v}\left(\vec{r}\right)\rho^c\left(\vec{r}\right)\frac{\partial^2 V_{XC}}{\partial \rho^2}\Big|_{\rho^v(\vec{r})} \tag{17}$$

For this difference to be significant, two things are needed: that ρ^v and ρ^c overlap (otherwise $V_{XC}\left(\rho^v\left(\vec{r}\right) + \rho^c\left(\vec{r}\right)\right) = V_{XC}\left(\rho^v\left(\vec{r}\right)\right) + V_{XC}\left(\rho^c\left(\vec{r}\right)\right) \forall\ \vec{r}$), and that the overlapping part of ρ^v changes significantly between the atomic and the production calculation (i.e $\exists\ \vec{r} \mid \Delta_{\rho^v}\left(\vec{r}\right), \rho^c\left(\vec{r}\right) \neq 0$). If those conditions are met and one unscreens using (13), the PP is not correct in a modified valence configuration. A prototypical case is the Cobalt PP , where the valence 3 d electrons strongly overlap with the 3 s and 3 p semicore electrons, and are strongly affected by bonding and magnetisation. (see section 4.5)

[3]The following discussion stands in the case of a semilocal or local XC functional -GGA or LDA ; unscreening in an exact exchange PP generation scheme, where the effect of the core density is nonlocal, is a much more complicated issue; see for example [12].

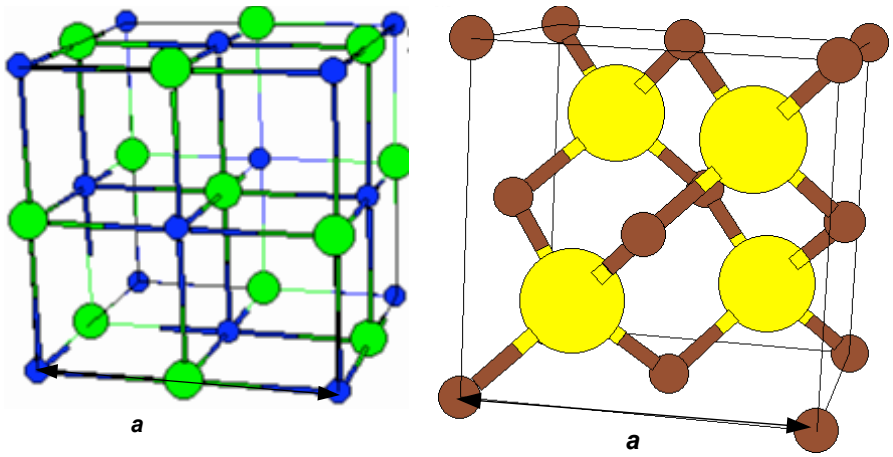

(a) (b)

Figure 1: Illustration of rocksalt (left) and zincblende (right) structure

As the full core density would need many plane waves to be described and only the part that overlaps with the valence density influences the calculation, one usually stores only a partial core density, with a given radius above which the exact core density is stored, and below which it drops in a smooth manner. This radius we will name core correction radius or NLCC radius.

2.4 Structures

A short rehearsal of the three structure we consider for II-VI compounds will be presented here. Rocksalt and zincblende structures (Figure 1) are both face centered cubic (fcc) systems. Zincblende is a two-elements analogue of the diamond structure, and has tetragonal coordination. Rocksalt has sixfold coordination. Both are described by one single parameter, the lattice parameter (a). Their unit cells both contain only two atoms (one of each element). The Brillouin zone of the fcc space group has body centered cubic (bcc) symmetry, as shown in Figure 2.

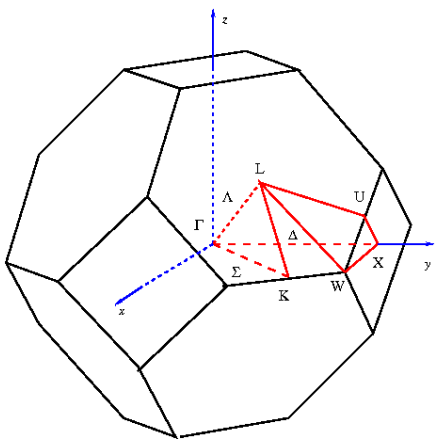

Figure 2: Illustration of the Brillouin zone for fcc systems, with high symmetry points and lines

The wurtzite structure (Figure 3) is the hexagonal analogue of zincblende; it is derived

from the hexagonal close packed (hcp) structure in the same way as zincblende is derived from fcc structure. It thus also has tetragonal coordination, and is similar to the "hexagonal diamond" structure. It has three degree of freedom ; a common choice of parameter, which we will use, is the set a (lattice constant), c/a and $u = g/c$ (displacement parameter [4]). The unit cell of wurtzite contains 4 atoms. The corresponding Brillouin zone is shown in Figure 4.

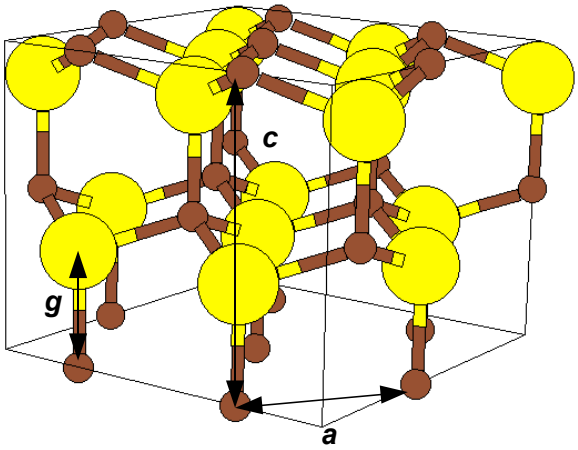

Figure 3: Illustration of wurtzite structure, with structural parameters

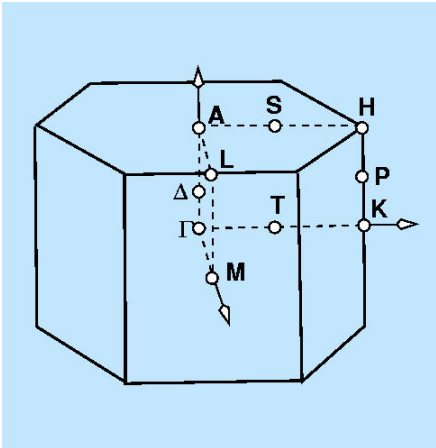

Figure 4: Illustration of the wurtzite Brillouin zone, with high symmetry lines and points

2.5 p-d mixing

An obvious difference between Zn and Mg compounds is the presence of occupied d-states in Zn. An extensive study of the role of d states in II-VI materials is presented in Ref. [63] ; we will shortly present here the mechanism of p-d mixing, which impacts our calculation the most. In tetrahedral structures (like zincblende and wurtzite), even and odd angular

[4]The wurtzite structure can be considered as two hcp lattices with the same a and c parameters, one for each atom type. The u parameter then quantifies the displacement between those two lattices, whence it's name.

momenta can hybridise. In zinc chalcogenides, such a mixing occurs between the anion (p) derived and the thrice-degenerate t_2 d derived states (while the twice degenerate e state is unaffected). This lead to several effects:

- The valence p band is moved up in energy, thus narrowing the gap
- The t_2 energy is lowered, putting it below the e states
- The p states acquires an antibonding character, leading to bigger lattice constants

Following Ref. [63], we will estimate the strength of this effect semiquantitatively using the perturbative formula:

$$\Delta E_{pd} = \frac{V_{pd}^2}{\epsilon_p^a - \epsilon_d^c} \text{ with } V_{pd} \propto \frac{r_d^{3/2}}{l_{bond}^{7/2}} \tag{18}$$

ϵ_p^a and ϵ_d^c being respectively the eigenvalues of anion p and cation d states, r_d being the d orbital radius and l_{bond} the average bond length. r_d does not vary amongst Zn compounds, thus the major differences come from $\frac{1}{(\epsilon_p^a - \epsilon_d^c)}$ and $\frac{1}{l_{bond}^7}$.

3 Methods

3.1 Supercell approach

The use of a plane wave basis set implies a periodic system; in normal bulk calculation the natural choice is to use periodic images of the elementary cell. In two case we will use different, bigger cells usually denoted as "supercells". For atomic and molecular calculations, the system of interest is placed in a big, essentially empty cell, whose size is sufficient for the mutual influence of periodic images to be negligible. For calculations implying impurities (or dislocation) in a solid, one uses a supercell made of many repetitions of the elementary cell (i.e. $3 \times 3 \times 2$ for our calculation of ZnO with Co impurity) with the correct modification to obtain an appropriate concentration.

3.2 Code

The code used to make our calculation is the PWSCF (Plane Wave Self-Consistent Field) package[5], which is part of the "Espresso" package. For SIC all-electron calculations on atoms, we used the "Atomic" code, which is part of the same package. Pseudopotentials were generated using the Fritz-Haber Institut code fhi98PP [16, 18, 29, 56].

3.3 Ionic structure relaxation

Once the electronic structure for a configuration is known , one is able to calculate forces acting on atoms using the "force theorem" (or Hellman-Feynman [13, 22] theorem), which states that for an an electronic wavefunction which is a minima of a given ionic configuration, the only energy derivatives to be taken into account are the explicit variation of the electronic Hamiltonian upon displacement of the atom, and the ion-ion interaction. It is in fact a special case of the generalised force theorem (Eq. (6) on page 5), considering the ionic positions as parameters.*i.e.*

[5] http://www.pwscf.org/

$$\vec{F_i} = -\frac{\partial E}{\partial \vec{R_i}} = -\langle\psi|\frac{\partial \hat{H}}{\partial \vec{R_i}}|\psi\rangle - \frac{\partial E_{II}}{\partial \vec{R_i}} \tag{19}$$

With $\vec{F_i}$ the force acting on an ion, $\vec{R_i}$ the position of this ion, and E_{II} the energy from the mutual interaction of ions

Thus the ionic structure can be relaxed with the use of a new SCF calculation for each ionic step. We use a damped Verlet [59] algorithm to converge the ionic structure. In this work, this approach was used for diatomic test molecules and for bulk structure having more than one free parameter (*i.e.* wurtzite and hexagonal close packed (hcp)). In these cases, a variable-cell relaxation was used to obtain an approximate structure. Then Murnaghan (see below) fits were produced by varying the lattice constant only, in order to obtain the equilibrium volume and the bulk modulus (K). To assess the accuracy of this procedure in the case of wurtzite, a murnaghan fit was produced for MgSe by adjusting c and u for each unit-cell volume; differences in energy, volume and K were so small that applying this time-consuming procedure to other materials was deemed unnecessary. For bulk system with one free parameter (such as rocksalt and blende structure), Murnaghan fits were used without resorting to relaxation.

3.4 Murnaghan's equation of state

While working on bulk material, a very useful equation is Murnaghan's [43] equation of state (equation 20 according to [14]), which allows to determine bulk modulus, lattice constants and total energy by a regression on calculations of total energy (E_T) for several unit cell volumes.

$$E_T(V) = E_T(V_0) + \frac{B_0 V}{B_0'}\left(\frac{\left(\frac{V_0}{V}\right)^{B_0'}}{B_0' - 1} + 1\right) - \frac{V_0 B_0}{B_0' - 1} \tag{20}$$

With B_0 and B_0' respectively the bulk modulus and its pressure derivative at equilibrium volume, $E_T(V)$ the total energy for one unit cell volume and V_0 the equilibrium unit-cell volume.

3.5 Band structures and projected densities of states

For PBE calculations, we will plot band structures from non-self-consistent field calculations (NSCF) based on the electronic density originating from SCF calculation and considering the k-points on the high-symmetry lines of interest. For hybrid XC functionals, NSCF calculation on an arbitrary set of points is not yet implemented in the code we use, thus eigenvalues are only available for points on the Monkhorst-Pack [42] grid used for SCF calculation. We thus identified on this grid values on high-symmetry lines of interest and obtained coarse band diagrams.

While producing band diagrams, we are considering Kohn-Sham states as reproducing electronic properties. This is a debatable procedure : in the Kohn-Sham *ansatz*, a mapping is done between the density of electrons and non-interacting fermions, thus the density is meant to be similar between the true and the model system. It is *not* assumed nor required that eigenvalues or dispersions should be well reproduced. However, from the Hohenberg-Kohn theorems, even excitations are uniquely defined by the ground-state

electronic density, and thus can be constructed from the Kohn-Sham density. Using Kohn-Sham states is one (reasonable) way to do so, which lives or dies depending on how reliable its results are.

We compute projected density of states (PDOS) using atomic wavefunction orthogonalized according to Löwdin's scheme [35]. When PDOS is presented along with a band diagram, it is computed on the set of k-point appearing in the band diagram, with equal weighing, otherwise it is computed on the Monkhorst-Pack grid.

4 Generating and testing pseudopotentials

For magnesium, oxygen and sulphur, we used pre-existing pseudopotentials, which we tested. For selenium and cobalt, we generated pseudopotentials on our own and select parameters in order to reproduce correct properties at reasonable costs. For zinc, we used at first an existing pseudopotential, which had already been thoroughly tested. When we moved to semi-empirical modification, we generated our own in order to control parameters.

4.1 Magnesium

The magnesium PP treats only the 2 s electrons as valence and was tested by simulating bulk metallic Magnesium, which has the hcp structure, at the PBE level; structural properties (table 1) were deemed acceptable for GGA DFT; the good reproduction of structural properties of magnesium chalcogenides was considered a further test. (Section 5.1)

Magnesium	a lattice [Å]	c/a []	K [Gpa]
Calculation	3.208	1.625	38.1
Experimental [5]	3.209	1.624	45.0
Relative difference	-0.04%	0.06%	-15.33%

Table 1: Computed and experimental properties of magnesium metal

4.2 Zinc

For Zinc, the first pseudopotential was generated according to the input file provided in the database of FHI code [4], using no core corrections and treating $3d$ and $4s$ electrons as valence. This PP has two features which can be questionable in terms of accuracy : the maximum of the d radial wavefunction is somewhat further away from the nucleus than in the all-electron calculation (fig. 6), because its peaked nature makes it expensive to describe using plane waves, and it includes no core corrections, even though the Zn(d) orbitals do overlap with the 3 s and 3 p semicore orbitals (fig. 5). A potential with a tighter convergence radius (1 bohr instead of 2) for d bands and reasonable core corrections (NLCC radius of 1 bohr) was generated. Quick tests showed that the d depth – our main issue (see Section 6.2) – was unaffected by these changes, and other changes were negligible. On the other hand, the tremendous increase in energy cutoff required by this PP made it unsuitable for all application beyond binary compounds, as these application are at the brink of computational affordability even with our softer PP. The negligible impact of NLCCs could be surprising, but is explained by the fact that d orbitals are only marginally

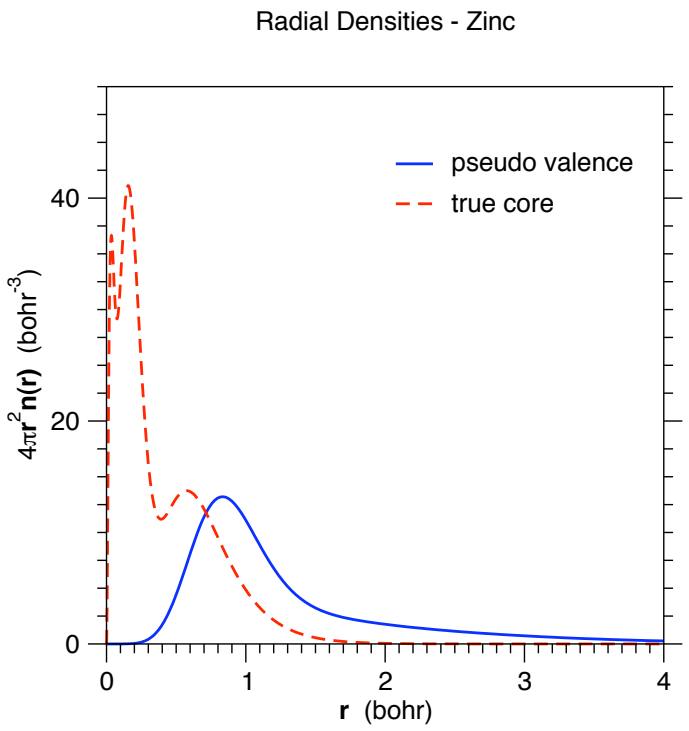

Figure 5: Core and valence densities in the zinc atom

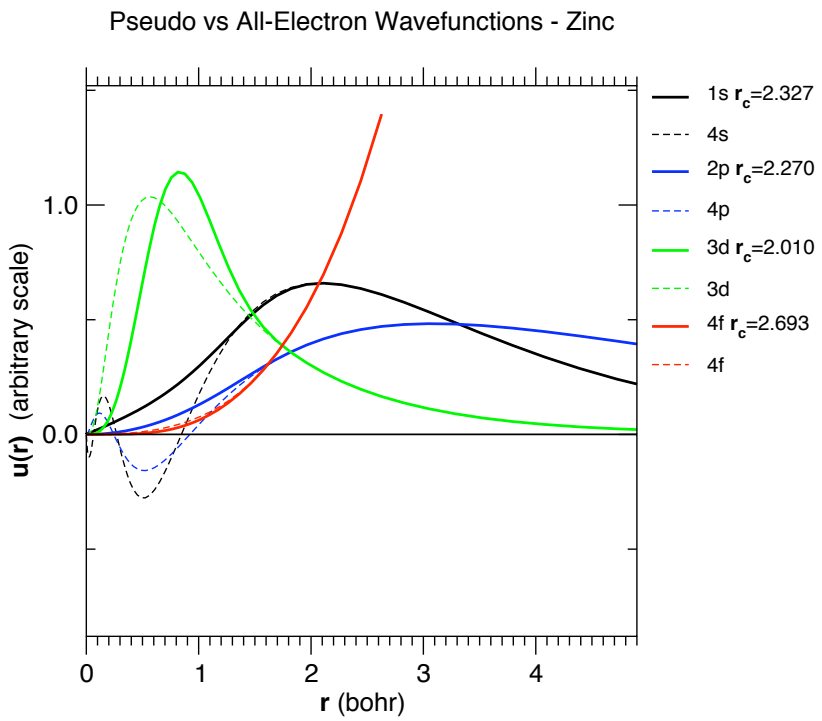

Figure 6: All-electron and pseudo wavefunctions of zinc. r_c: convergence radius

affected by the chemical environment.

Considering the heavy cost and little use of a harder PP, our standard, self-generated PP was the starting point for here presented PP modification (6.3) – even though such modification was first attempted with our harder PP, with no significant change at the PBE level.

4.3 Oxygen and sulphur

In order to test our pseudopotentials for oxygen and sulphur as well as to investigate the effects of PBE0, we first simulated three diatomic molecules: O_2, S_2 and SO. We compared (Tables 2, 3 and 4) their bond length (L) as well as their dissociation energies to experimental data (corrected for zero point vibration according to data in Ref. [26], established using eq. (21)) from the book by Huber and Herzberg [25]. Dissociation energies were computed by comparing energies of molecules with energies of their separated constituents in their fundamental state.

$$ZPE = Y_{00} + \frac{\omega_e}{2} - \frac{\omega_e x_e}{4} \text{ with} \tag{21}$$
$$Y_{00} \simeq \frac{B_e}{4} + \frac{\alpha_e \omega_e}{12 B_e} + \frac{\alpha_e^2 \omega_e^2}{144 B_e^3} - \frac{\omega_e x_e}{4}$$

with ω_e the harmonic frequency, $\omega_e x_e$ the first anharmonicity constant, and B_e and α_e rotational constants.

Our PPs for all VI atoms treat the outermost 6 electrons as valence, other electrons being included in the core. As can be seen, agreement with experimental values is quite good. PBE0 provides an improvement for binding energies but not always for bond length; it inverses the trend of PBE to predict too stretched bonds.

O_2	L [Å]	$\frac{\Delta L}{L}$[%]	Binding energy [eV]
PBE	1.218	0.91	5.87
PBE0	1.193	-1.21	5.56
Exp. [25]	1.208	/	5.21

Table 2: O_2 molecule; $\frac{\Delta L}{L}$ is the relative deviation of the bond length with respect to the experimental value

S_2	L [$\mathring{A}$]	$\frac{\Delta L}{L}$[%]	Binding energy [eV]
PBE	1.906	0.91	4.90
PBE0	1.882	-0.395	4.71
Exp. [25]	1.889	/	4.41

Table 3: S_2 molecule

4.4 Selenium

During the production of the selenium pseudopotential, we examined two parameters: the inclusion of a partial core density (section 2.3.1), and the inclusion of a f channel in the

SO	L[$\AA$]	$\frac{\Delta L}{L}$[%]	Binding energy [eV]
PBE	1.498	1.15	5.90
PBE0	1.474	-0.5	5.64
Exp. [25]	1.481	/	5.43

Table 4: SO molecule

PP. Our test systems were SeO and SeS, using experimental data from [25]. Binding energies corrected for zero-point energy according to equation (21) from Ref. [26] .

SeO					
PP	Functional	Bond length [A]	$\frac{\Delta L}{L}$	Binding energy [eV]	$\frac{\Delta E}{E}$
No core corrections	PBE	1.662	0.85%	5.19	16.40%
	PBE0	1.634	-0.83%	4.34	-2.52%
NLCC radius =1.0 bohr	PBE	1.658	0.62%	5.22	17.07%
	PBE0	1.633	-0.89%	4.46	0.00%
NLCC radius =0.9 bohr	PBE	1.658	0.62%	5.22	17.04%
	PBE0	1.633	-0.88%	4.46	-0.02%
NLCC radius =0.9 bohr, no f	PBE	1.687	2.39%	4.88	9.61%
	PBE0	1.665	1.04%	4.17	-6.42%
Experimental [25]	/	1.648	/	4.46	/

Table 5: SeO molecule

The result for SeS and SeO with various pseudopotentials are available in Tables 5 and 6. As can be seen, the addition of core corrections greatly diminished the overestimation of the SeS binding energy at the PBE0 level; interestingly it also corrected the SeO under-binding, which confirms that it leads to a better description. As can be seen, a reference radius of 1 bohr is small enough, as further reduction of it doesn't affect results notably. Electronic density of the all-electron core, chosen pseudocore and valence electrons cand ben seen in figure7 . It was also shown that including a f channel was needed, as its absence leads significant changes in both structure and energies. This could originate in the fact that we used the f channel as local part of the PP, and replacement of it by the d channel leads to changes.

4.5 Cobalt

For the cobalt pseudopotential, where $3d$ and $4s$ electrons were treated as valence, tests were run on metallic cobalt, which has the hexagonal close packed structure. We looked at its structural properties as well as at the magnetisation. Results for various reference radius for the partial core density are shown in table 7. As can be seen, the inclusion of core corrections is vital here, which is not surprising as the valence $3d$ density overlap markedly with the semicore $3s$ and $3p$ density, as can be seen on figure 8. A pseudo-core reference radius of 1 bohr was found to give sufficient convergence of structural and magnetic properties.

SeS					
PP	Functional	Bond length [A]	$\frac{\Delta L}{L}$	Binding energy [eV]	$\frac{\Delta E}{E}$
No core corrections	PBE	2.054	0.89%	4.79	28.14%
	PBE0	2.027	-0.43%	4.72	26.36%
NLCC radius =1.0 bohr	PBE	2.051	0.76%	4.80	28.61%
	PBE0	2.028	-0.39%	4.08	9.20%
NLCC radius =0.9 bohr	PBE	2.052	0.76%	4.80	28.65%
	PBE0	2.028	-0.39%	4.08	9.21%
NLCC radius =0.9 bohr, no f	PBE	2.065	1.40%	4.61	23.45%
	PBE0	2.044	0.41%	3.96	5.91%
Experimental [25]	/	2.036	/	3.73	/

Table 6: SeS molecule

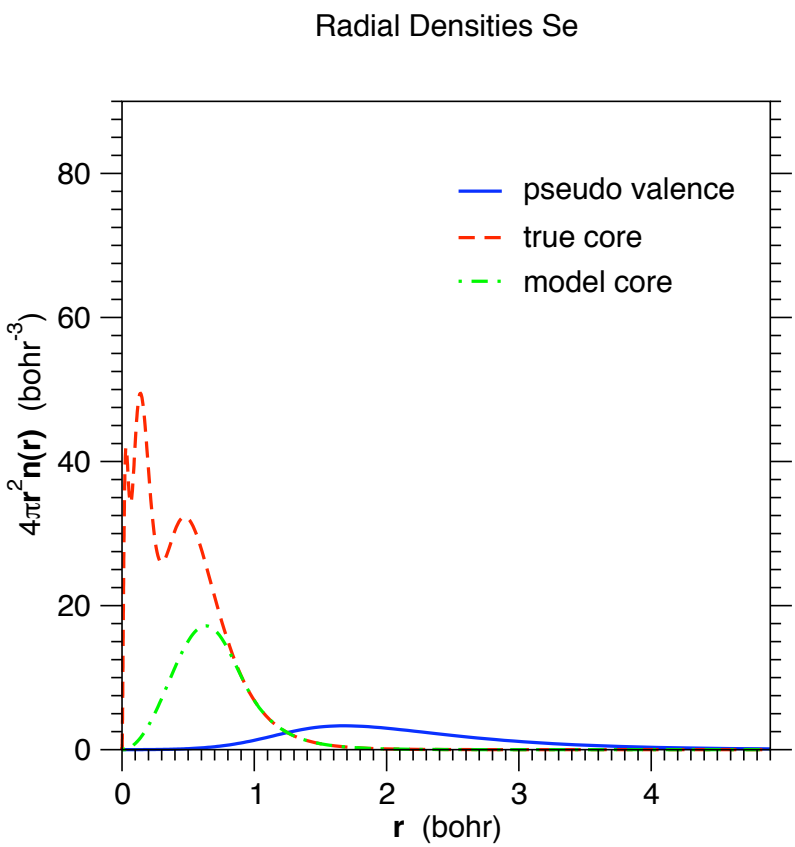

Figure 7: Valence, core and pseudocore radial density for selenium; pseudocore for a reference radius of 1 bohr

NLCC radius [bohr]	a [Å]	c/a	magnetization [$\mu_{bohr}/cell$]	K [GPA]
No CC	2.525	1.793	5.09	not computed*
1.2	2.487	1.613	3.71	209.38
1	2.485	1.611	3.6	216.89
0.8	2.485	1.611	3.6	219.72
experimental	2.507 [5]	1.623 [5]	3.35 [55]	194.9 [52]

Table 7: Calculations on bulk cobalt; *other properties were blatantly not correct, thus no Murnaghan fit was produced using this PP

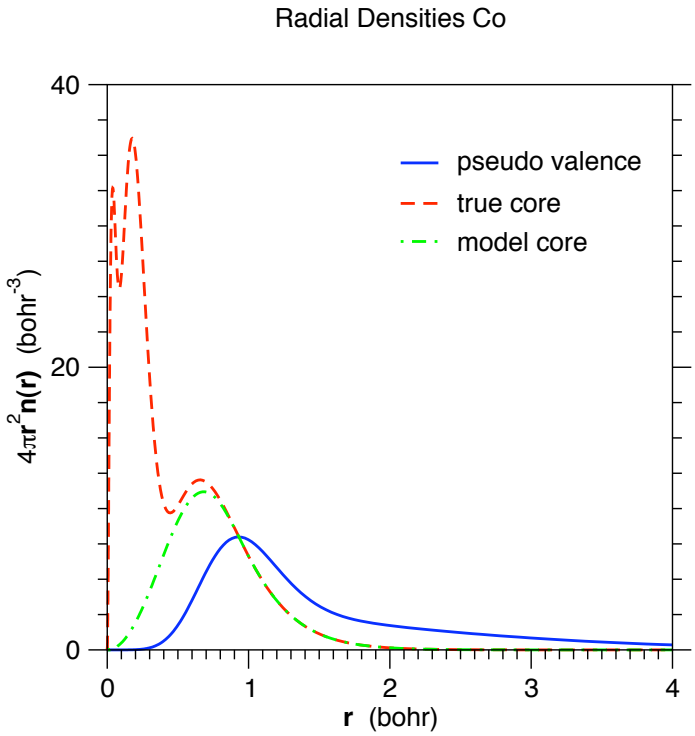

Figure 8: Valence, core and pseudocore radial density for cobalt; pseudocore for a reference radius of 1 bohr

5 Magnesium Chalcogenides

5.1 Structures and relative stability

We will start our discussion of structural properties of magnesium chalcogenides with MgSe, as difficulties encountered while studying it were a motivation to more extensive study of the different phases of magnesium chalcogenides than was initially devised. MgSe has been reported in three different structure. Rocksalt [41] is usually considered the equilibrium structure; wurtzite was reported as a long-lasting metastable phase [41] , and zincblende , though not stable [19], is often considered as the limit of tertiary or quaternary compounds containing magnesium, zinc and selenium, as those tend to adopt this structure. Various experimental properties of these structures are listed in Table 5.1.

Experimentaly determined structures for MgSe				
Source	structure	E_{gap} [eV]	lattice constant [Å]	Stability
[41]	Wurtzite	/	4.15	metastable
[2]	Rocksalt	/	5.45	stable
[10]	Rocksalt	/	5.463	stable
[36]	?	4.05	/	/
[27]	Rocksalt	3.9	5.46	stable
[33]	ZincBlende	4.05	5.904	less stable than RS
Extrapolations from ternary/quaternary compounds				
[44]	Zincblende	3.6	5.89	not stable
[19]	Zincblende	3.6	5.89	not stable
[51]	Zincblende	4.1	5.964	not stable
[61]	Zincblende	3.85	5.89	not stable
[27]	Zincblende	4.0	5.91	not stable

Table 8: Reported structures and band gaps of MgSe

It should be noted that there are frequent confusion in the literature between the different structures, with lattice constant from zincblende being given as rocksalt([8]) and *vice-versa*, extrapolated gap for zincblende being given as rocksalt gap, etc. In those conditions, it was deemed necessary to study all three structures at both the PBE and the PBE0 level. We studied the relative stability of MgO and MgS structures at the PBE level, in order to determinate how PBE performs in predicting the relative stability of those structures.

For MgSe, PBE and PBE0 murnaghan fit (Figures 9a and 9c) were computed for cubic structures. For the wurzite, structure was optimised using the PBE XC functional. As a full Murnaghan fit would be computationally too demanding using PBE0, the u and c/a parameter from the PBE calculation were kept, and the a parameter was chosen such as to obtain the same volume per elementary formula as for the zincblende PBE0 optimal structure, a reasonable procedure in regard of the similarities of these structures and of the PBE case.

For both functionals , wurtzite was found to be the most stable phase, closely followed by zincblende, with rocksalt being the least stable of the considered phases. These result should be considered with caution in view of the small energy differences (smaller than 0.1 eV). Comparison of our calculation with available experimental data is presented in table 5.1.

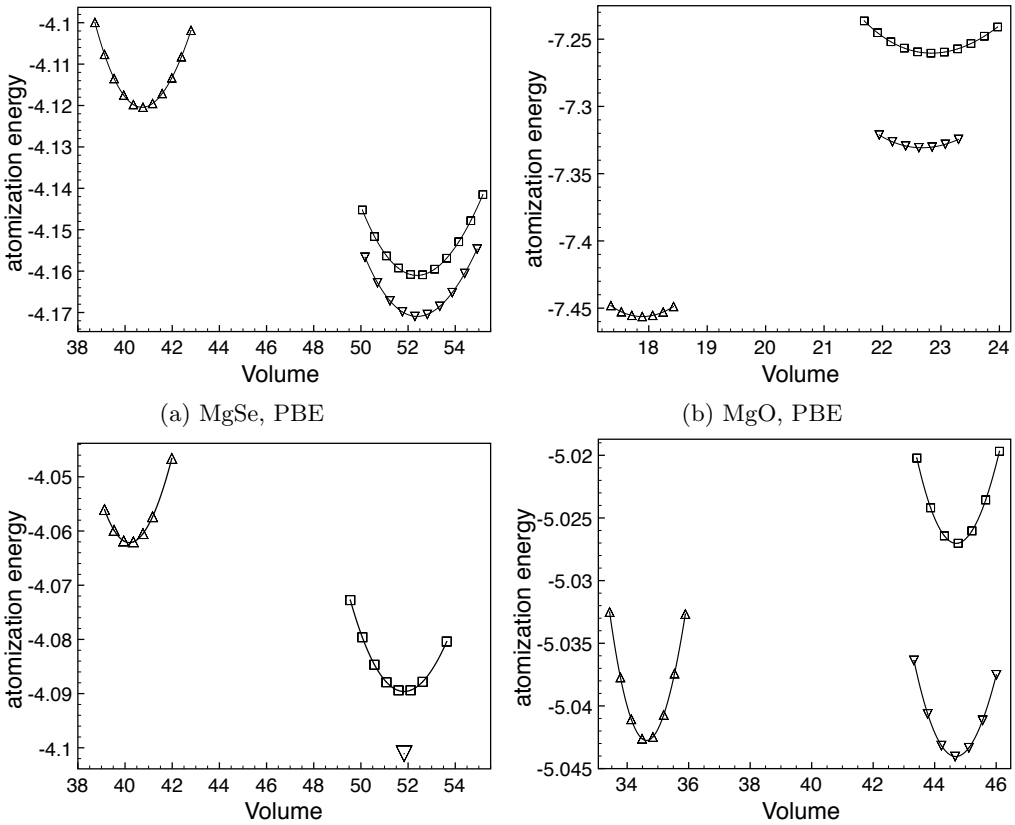

(a) MgSe, PBE

(b) MgO, PBE

(c) MgSe, PBE0

(d) MgS, PBE

Figure 9: Energy vs volume plots for the three considered structure of the three magnesium compounds. $\triangle$: rocksalt; $\bigtriangledown$: wurtzite; squares: zincblende. Lines: murnaghan fits. Volumes in Å^3 per elementary formula, atomisation energies in eV per elementary formula. Atomization energies are obtained by substracting the isolated atoms energy in order to have values more convenient than the total energy, but are not meant to be rigourously defined.

Structure	a lattice [A]			K [GPA]		Gap [eV]		
	exp.	PBE	diff. %	exp.	Comp.	exp	PBE	PBE0
Blende	5.91	5.94	0.49 %	/	45.8	4.05 [33]	2.58	4.42
Rocksalt	5.46	5.45	-0.27 %	/	66.9	3.9 [27]	1.78	3.44
Wurzite	4.15	4.21	1.68 %	/	45.7	(4.05)	2.6	4.47

Table 9: Comparison of experimental data with our calculation for three MgSe structures; no value of the gap was found for wurtzite, but it should be close to the similar zincblende.

Taking the measures from refs. [27] and [33] as reference points, we notice that, using PBE0, the gap is underestimated in the rocksalt phase and overestimated in the zincblende phase, which leaves little hope of achieving a good description of both phase with the same alpha parameter. Such a different behaviour between two structures of a same compound remains to be explained.

In the case of MgO (Figure 9b), DFT correctly predicts the rocksalt structure to be the most stable, while for MgS (Figure 9d) wurtzite and rocksalt are almost isostable. Wurzite is a known metastable phase of MgS [41], with a = 3.972 Å, in accord with our computed value of a = 4.005 Å. We observe three general trends: our calculations tends to favour wurzite (and likely zincblende) too much over rocksalt, tetragonal structure become more favoured as the atomic number of the cation increases (as it should ; MgTe is stable as wurzite), and wurzite is more stable than zincblende for all those compounds. The latter observation is consistent with the fact that in ref. [41], MgS and MgSe wurtzite were obtained from the amorphous phase, rather than zincblende.

		Lattice constant[$\AA$]	K [GPa]
MgS	calc.	5.174	74.5
	Exp.	5.203 [11]	78.9 ±3.7 [46]
MgO	calc.	4.152	155
	Exp. [8]	4.216	164

Table 10: Comparison of PBE calculation with experiment for MgS and MgO rocksalt

5.2 Electronic structure

We now study the electronic structure of those compounds. In order to compare similar cases, from now on we consider only the rocksalt structure, which is experimentally the most stable for all three materials. We present projected density of states (PDOS) and band diagrams for all three materials in figures 10, 11 and 12. This allows us to determine the main caracter of the different bands. The upper part of the valence band is mainly derived of anion p states (a deep band of anion s character is present but not shown in our diagrams). The conduction band minimum (CBM) is mostly made of cation s character, as can be expected from the ionic picture, where the bonding is made by the transfer of 2 electrons from the magnesium to the anion, leaving Mg(s) states as (lowest) unoccupied states, and completely filling anion p bands. Bands will be hereafter named following their dominant character. In accord with experimental data, MgO is predicted to have a direct Γ gap, while MgS and MgO show indirect $\Gamma - L$ gap.

We also computed the band gap of magnesium chalcogenides using PBE and PBE0 on the PBE determined structure. The results are presented in Table 11.

$E_{gap}[eV]$	exp.	PBE	PBE0
MgO	7.70 [8]	5.11	7.67
MgS	4.6 [53]	2.77	4.63
MgSe	3.9 [27]	1.78	3.44

Table 11: Experimental and computed gaps for rocksalt Mg chalcogenides

As was expected, PBE underestimates the gap in all cases; PBE0 is correct for MgO

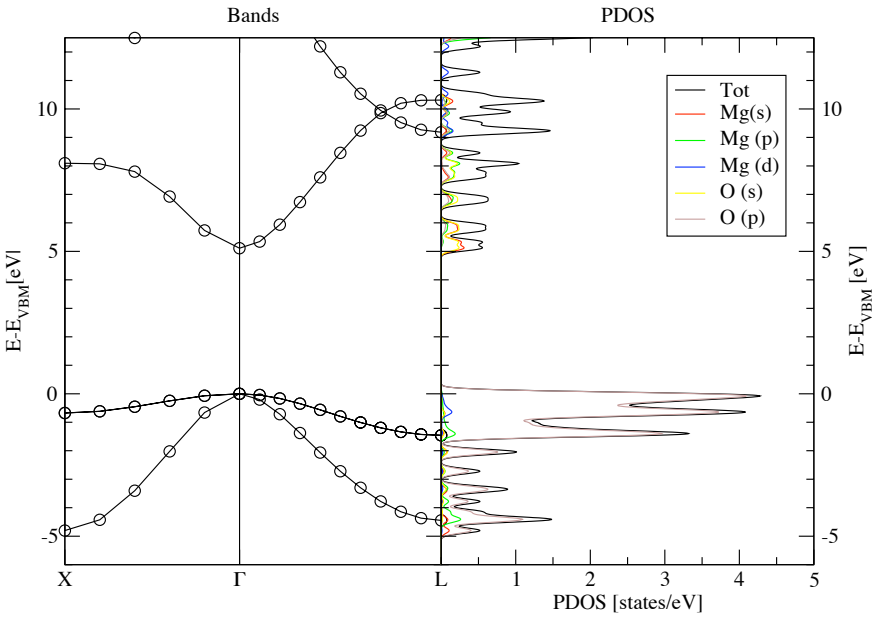

Figure 10: PBE band diagrams and projected densities of states for MgO

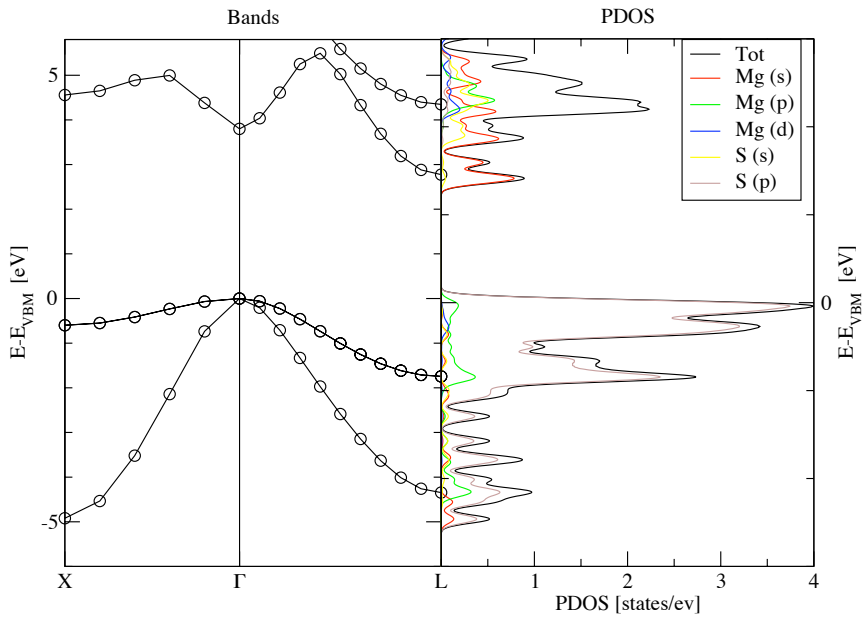

Figure 11: PBE band diagrams and projected densities of states for MgS

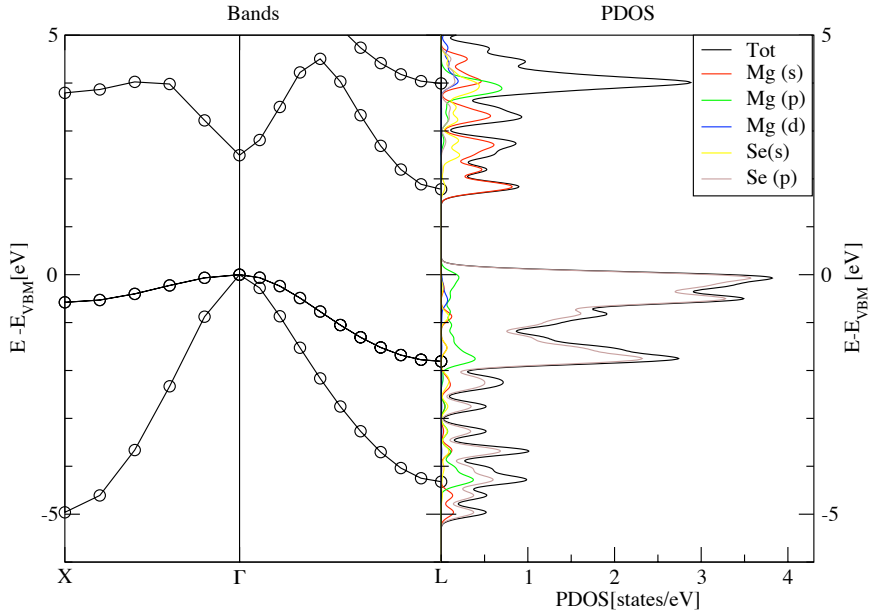

Figure 12: PBE band diagrams and projected densities of states for MgSe

and MgS, but underestimates the gap for MgSe. A next step was to study the relation between the alpha parameter and the electronic gap. A test study was run on MgO (figure 14), which shows a linear relationship. For further variation of alpha (including Zinc compounds), we used linearization from the PBE and PBE0 results, without bad surprise (results within 0.1 eV from what was expected; whenever an "optimised alpha" calculation is mentioned, consider it produces the experimental gap if there is no other indication).

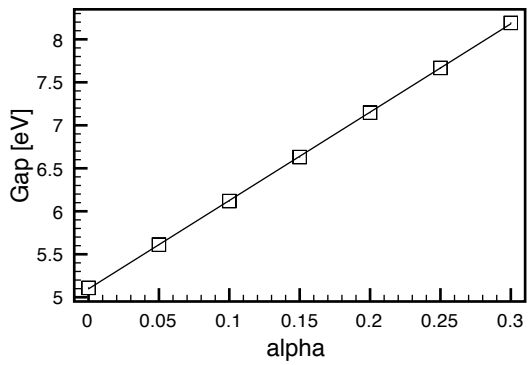

Figure 13: Dependence of MgO gap on the alpha parameter. Fit: $E_{gap} = (5.10+10.3\alpha)$ eV

We then tabulated (Table 12) the difference between the experimental gap and the PBE0 computed one, along with the Phillips ionicity [50] and the value of alpha that gives

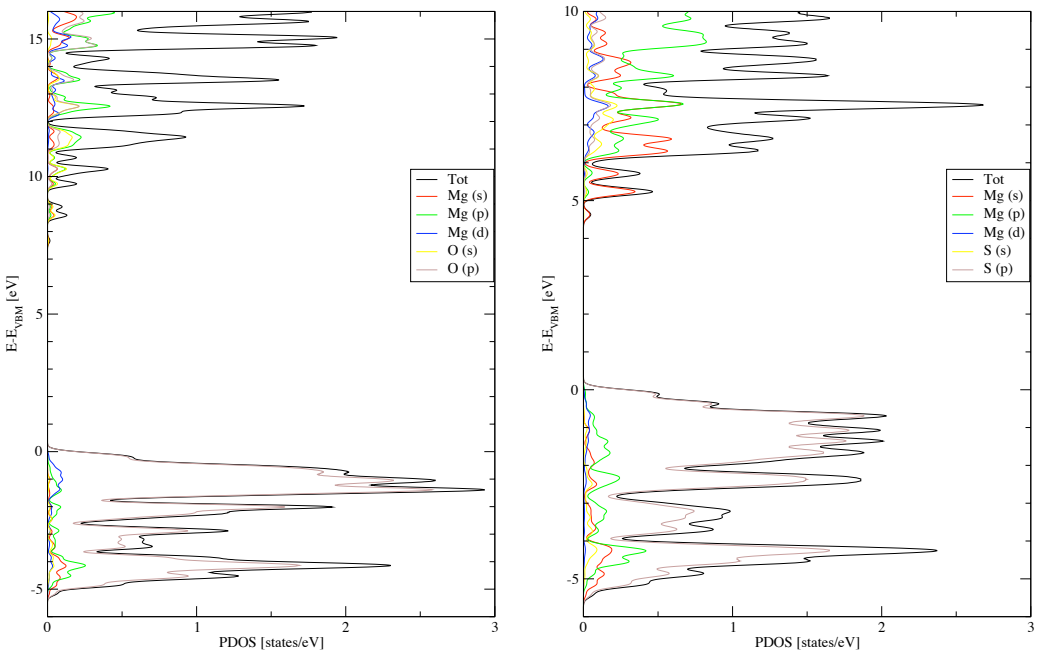

(a) (b)

Figure 14: PBE0 PDOS for MgO (left) and MgS (right)

the experimental gap. It is blatant that no relation between ionicity and other values

Compound	Δ_{gap}	philips ionicity [50]	optimised alpha
MgO	- 0.03	8.41	0.253
MgS	+0.03	7.86	0.246
MgSe	-0.46	7.90	0.316

Table 12: PBE0 error on the gap (Δ_{gap}) and *ad-hoc* α parameter vs ionicity for rocksalt MgX

can be derived. However, three cases is too few to establish (or dismiss) such a relation ; zinc compounds were to be included in that search, but they needed more than alpha adjustment for a correct description (*vide infra*). We also produced PDOS diagram using PBE0 for MgO and MgS (Figure 14), and using an *ad-hoc* α for MgSe (Figure 15).

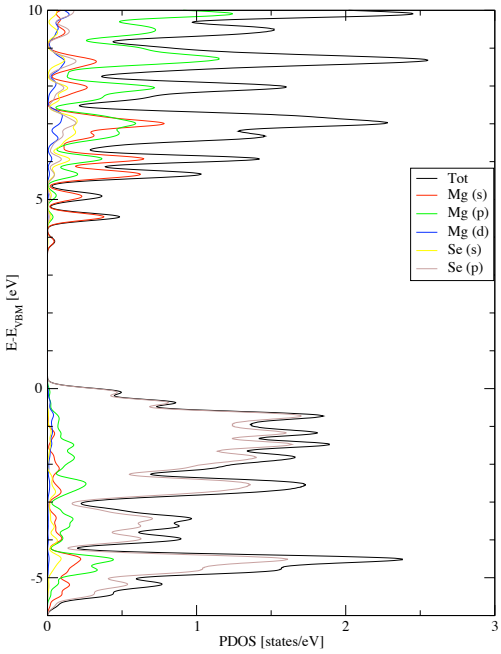

Figure 15: *Ad-hoc* α (=0.316) PDOS for MgSe

6 Zinc Chalcogenides

6.1 Structural properties using PBE

Structural properties were determined using the PBE XC functional, compared to their experimental counterpart, and found to be acceptably accurate. They will be presented later on in Table 17 along with the results for modified pseudopotentials.

6.2 Electronic properties using GGA and hybrid functionals

As for magnesium chalcogenides, we produced band diagrams and PDOS for all three compounds using PBE XC functional, which we present in Figures 16, 17 and 18. For comparison, they are placed along with their modified pseudopotential counterparts.

We then applied PBE0 to all three Zn compounds and computed the gaps and d-bands depth. That depth was determined by a weighted average on the density of states of the five (resp. ten for wurtzite, which has two elementary formula per unit cell) lowest lying bands . As can be seen in Table 13 , gaps are correct for ZnS and ZnSe but not ZnO, while d states lie too high in all cases. An optimised alpha calculation was made for ZnO in order to establish its effect on d bands as well as to reproduce the experimental gap (see table 14). It showed so little effect on d states that more than 100% exact exchange would be necessary to fix their position. Such an α would be inappropriate for the rest of the electronic structure (*i.e.* the gap). Examination of the corresponding PDOS diagrams (Figures 19, 20 and 21, as compared to Figures 16, 17 and 18) shows that exact-exchange doesn't shift d-bands significantly down in any of these compounds, and that it doesn't act notably on the amount of d character in p-bands either.

These results will need a detailed discussion, which will presented in the following part.

Compound	Exp.Gap	PBE0 Gap	Exp d-band depth	PBE0 d-band depth
ZnO	3.44	2.76	-8	-5.44
ZnS	3.78	3.64	-9.5	-6.78
ZnSe	2.75	2.78	-9.2	-7.14

Table 13: PBE0 results for zinc chalcogenides

Alpha parameter	band gap	d-band depth
0.000	0.772	5.006
0.250	2.758	5.441
0.347	3.49	5.64
Exp.	3.440	8.000

Table 14: Influence of the α parameter on electronic properties of zinc oxide

6.2.1 Analysis and comments

Our first assumption is that the d bands are badly positioned because of the self-interaction (SI) problem. As discussed in the theoretical section 2.2.3, the higher localisation of d states makes them more sensitive to SI, and thus too weakly bound.

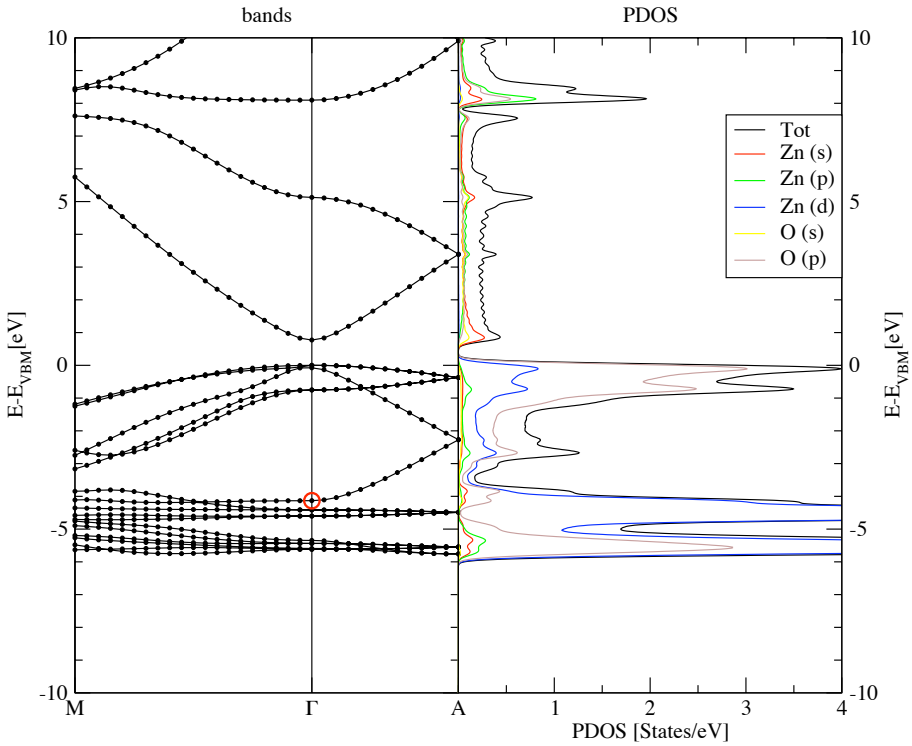

(a)

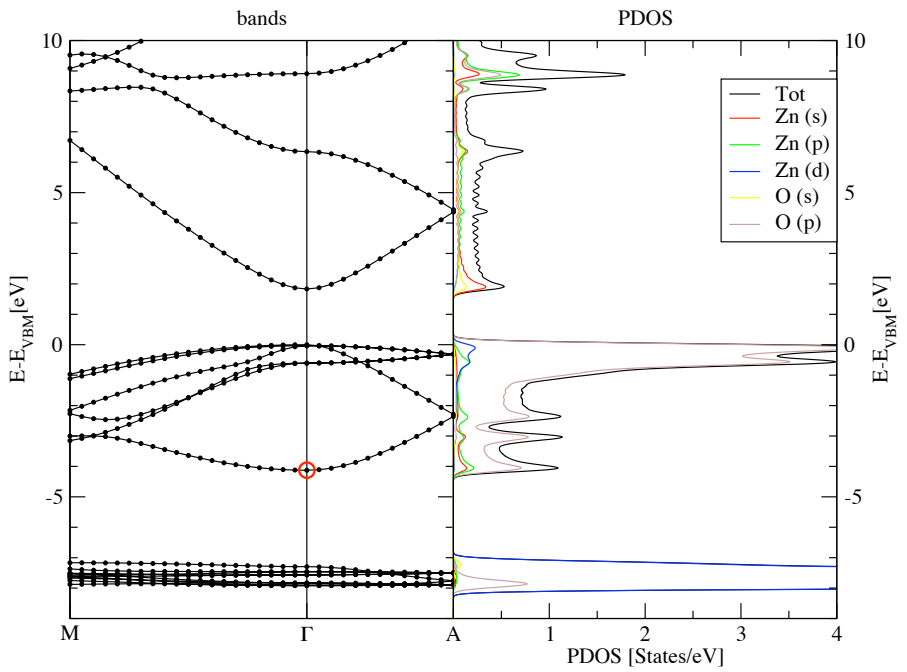

(b)

Figure 16: Band diagrams and projected densities of states for ZnO with original (top) and modified (bottom) PP. Red circled points: state whose contour plot is shown are Figure 22.

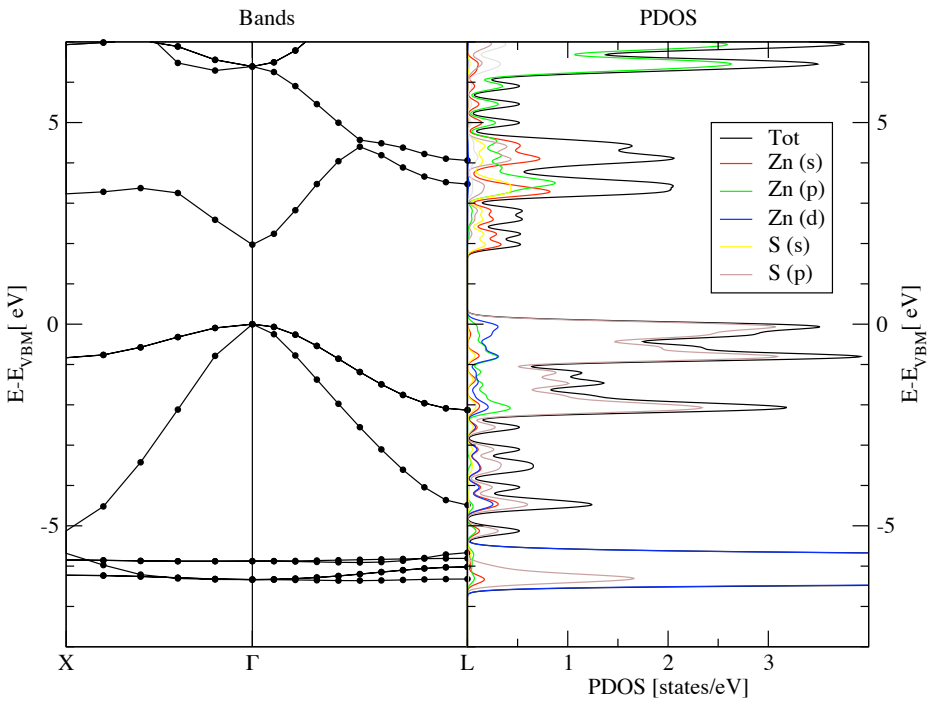

(a)

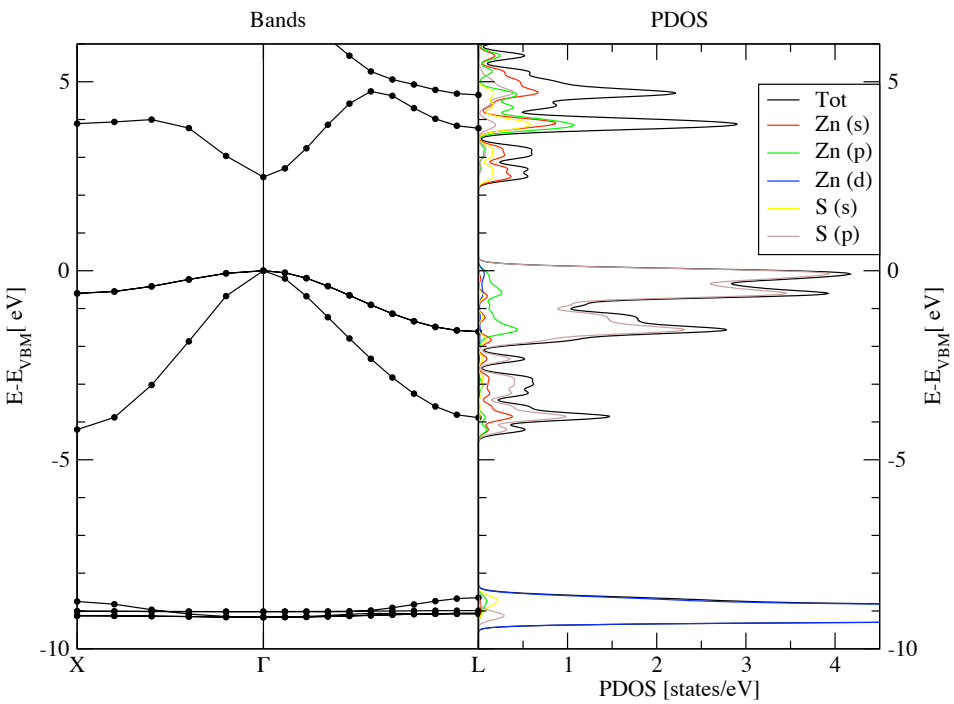

(b)

Figure 17: Band diagrams and projected densities of states for ZnS with original (top) and modified (bottom) PP

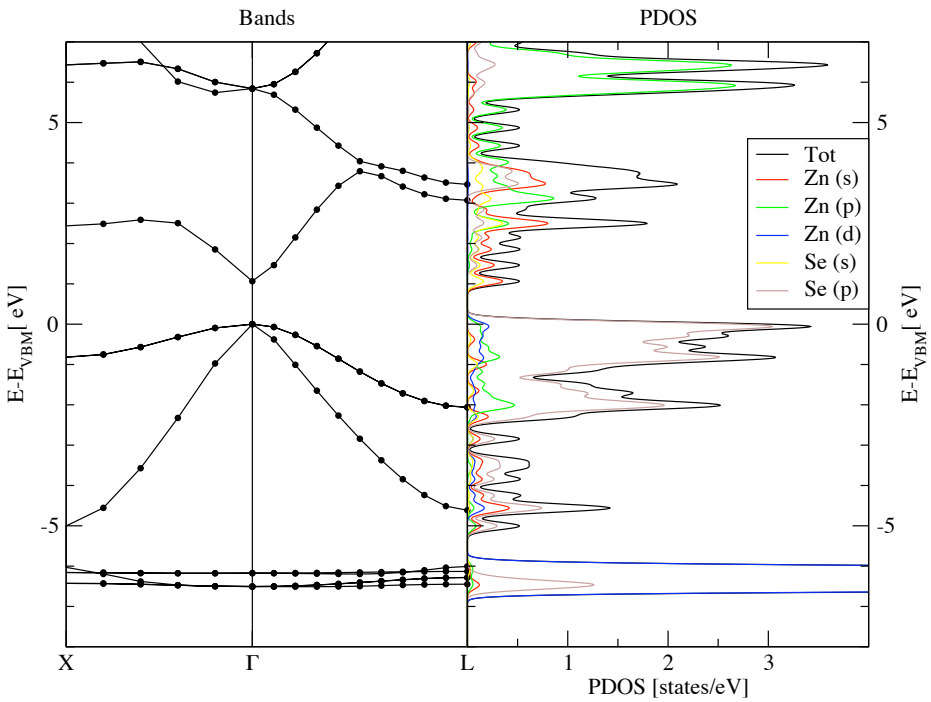

(a)

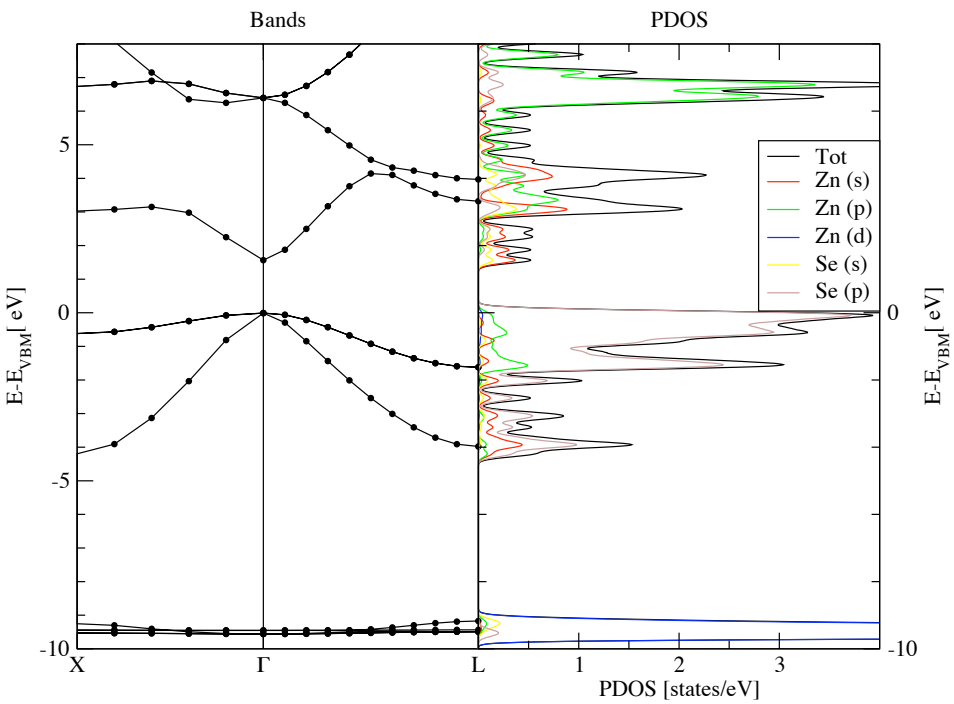

(b)

Figure 18: Band diagrams and projected densities of states for ZnSe with original (top) and modified (bottom) PP

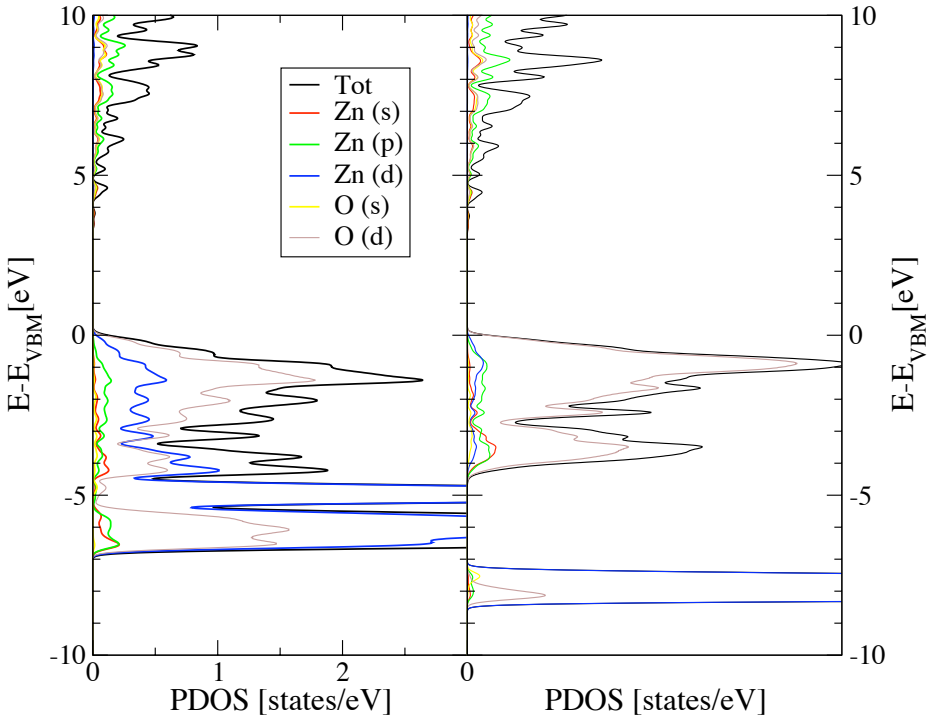

Figure 19: Projected densities of states for ZnO using hybrid XC functionals, with conventional (left) and modified (right) PP

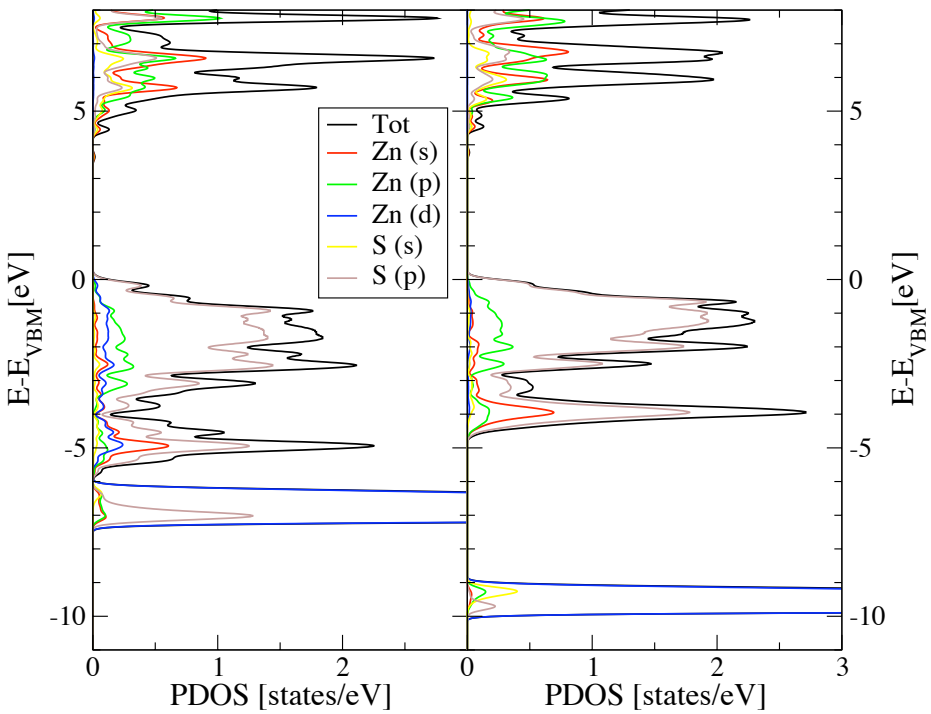

Figure 20: Projected densities of states for ZnS using hybrid XC functionals, with conventional (left) and modified (right) PP

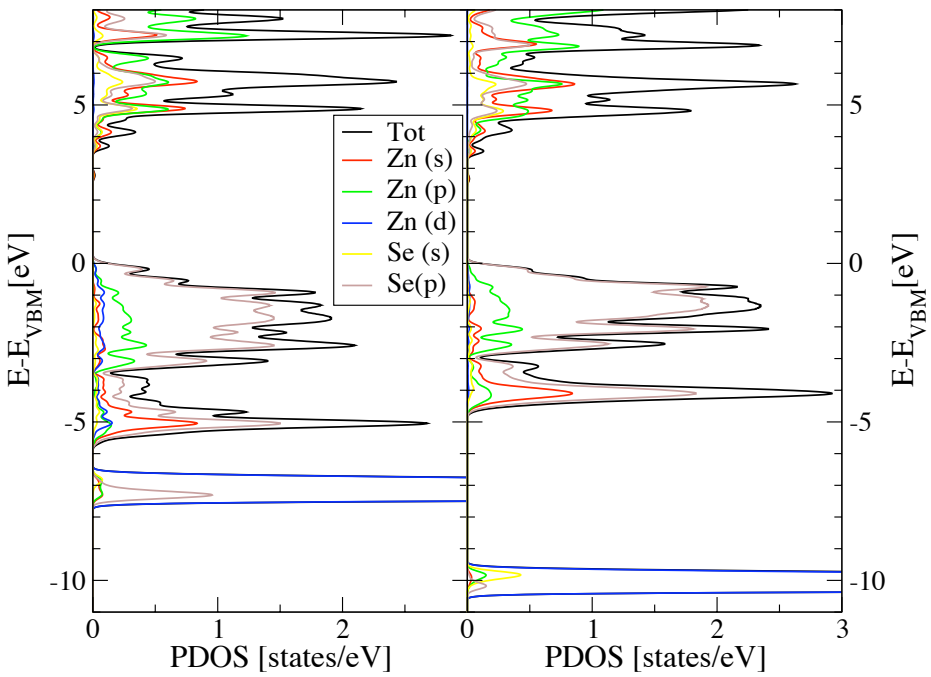

Figure 21: Projected densities of states for ZnSe using hybrid XC functionals, with conventional (left) and modified (right) PP

This bad description of d-bands is not without effects on the band gap, as explained in the "p-d mixing" section (2.5). As can be seen from eq. (18) on page 10, the higher the d-states lie, the higher the p bands and the narrower the gap is. However, d bands are too high in all three compounds, and only for ZnO is the gap underestimated. This can be explained by the relative magnitude of the p-d mixing; using eq. (18) with the values from our calculation, we get an estimate of the strength of this effect. ZnO has both the smallest l_{bond} and the highest d-bands in our calculation (see Table 15). We estimate $\epsilon_p^a - \epsilon_d^c$ by the depth of d-bands, [6], which leads to a much stronger p-d coupling and stronger influence of the position of d-bands on the gap[7] . This strong coupling in ZnO can also be seen

Compound	d	d^{-7}	$\epsilon_p^a - \epsilon_d^c$	$\frac{\Delta E_{p-d}}{\Delta E_{p-d,ZnO}}$
ZnO	2.003	0.0077	-5.44	1
ZnS	2.343	0.0026	-6.78	0.27
ZnSe	2.455	0.0019	-7.14	0.18

Table 15: Estimation of the strength of p-d coupling in zinc compounds

in our projected density of state calculations (Figure 16a; ZnO "p" bands have strong d character (almost as strong as p), this character is weak in ZnS (Figure 17a) and almost

[6] An estimation based on atomic eigenvalues as we calculate them would give even stronger p-d coupling in ZnO (see Table 16)

[7] Eq. 18 comes from a perturbative point of view, which is likely to break up in our calculation on ZnO, so that this discussion must be considered as essentially qualitative.

	Zn (d)	O (p)	S (p)	Se (p)
PBE	-10.05	-9.54	-7.19	-6.65
PBE0	-11.70	-11.62	-8.6	-7.93
PBE-SIC*	-21.14	-17.32	-11.77	-10.75

Table 16: Atomic eigenvalues for d and p orbitals of interest ; * using all electron calculation in "atomic" code, other case using PWSCF and our PPs

negligible in ZnSe (Figure 18a).

Thus, the ZnO gap is affected to a much stronger extent than are gaps for ZnS and ZnSe, however the bad d positioning should affect those as well, and thus the fact that PBE0 gives the correct gap is likely due to error cancellations. With these d-bands, ZnS and ZnSe *should* have underestimated band gaps. Taking these considerations into account, merely adjusting alpha to obtain the experimental gap –without correct d-bands– cannot be considered an accurate description of our systems.

Another fact needs commenting: if the d-bands are badly positioned because of the self-interaction problem, one could expect that adding exact exchange would have a strong effect on them. This expectation is also backed up by the fact that ref. [39] mentions a Hartree-Fock d-bands depth as low as -11.4 eV. However, as was shown, d bands depth is hardly affected by the addition of exact exchange. We propose that the use of PBE generated PPs is responsible for this ; our PPs are established without exact exchange, and as the most of the d wavefunctions is inside the core radius, their energy depends mostly on the pseudopotential, in such a way that including exact exchange in the bulk calculation only brings a slight correction to their depth relative to anion (p) bands.

In order to estimate the magnitude of the self-interaction error, we performed calculations of isolated atoms using our PPs with PBE and PBE0. On another hand, we used an all-electron calculation using PBE corrected for self interaction according to the scheme of [49]. Table 16 lists atomic eigenenergies for Zn (d) and anions (p). As expected, Zn(d) is the most sensitive to SIC, by several eV, confirming that at the atomic level SI underbinds d states the most. On the other hand, the PBE0 correction for Zn(d) is weak, even weaker than that for O(p), confirming the poor success of PBE0 in correcting the d-bands with the current PP.

Our assumption that a big part of the SI effect is enclosed in the pseudopotential is backed up by the fact that Vögel, Krüger and Pollmann [60] obtained a good description of both gaps and d-bands of several IIb-VI compounds by using SIC pseudopotentials along with standard LDA for the calculation in the solid.

6.2.2 Proposed solutions

In summary, zinc chalcogenides at the GGA level combine two problems: an underestimated gap originating from the lack of discontinuity at filled shells, and a bad positioning of d-bands due to the self-interaction problem. To treat these problems, several approach have been used or could be proposed:

- Adding extensive orbital-dependant *ad-hoc* corrections, either in the form of DFA+U (as inref. [62]) or non-local external potential (as in ref. [31]), in order to recover experimental properties
- Performing hybrid calculations in an all-electron scheme, in order to recover the full effect of exact exchange on d states.

- In the same spirit, generate PP specifically for hybrid functionals
- Use SIC PPs (see Ref. [60]), or full SIC calculation.

Some comments need be done on those approaches: *ad-hoc* corrections as in ref. [31] (which use one adjustable energy constant per orbital) allow to recover most desired properties, but are very system specific, thus they find only limited applications. Furthermore, they lack theoretical justification.
Performing all-electron calculations and generating hybrid PP are both too complicated and different from the scope of this work to be performed during the limited time devoted to this thesis. All-electron hybrid calculations using the B3LYP XC functional exist [6,45] and yields correct gaps. In ref. [6], structural values correspond to experiment but d-bands are about 4 eV deep, while in ref. [45] d-bands are about 6.2 eV deep in average, whereas the lattice constant is overestimated by about 4%.
SIC approaches pose transferability problems ([54]) which we won't comment here.

Our approach will be to perform an *ad-hoc* correction of the PBE PP to correct the position of d-bands, and to adjust the exact exchange to recover the experimental gap. This allows to adjust the energy of d states at no additional computational cost.

6.3 Modified pseudopotential approach and its effects

6.3.1 Principle and method

As was pointed out before, the effect of SI is enclosed in PPs, thus we will try to correct PPs in order to shift d-bands to a more realistic energy level. In order to do this, we will act on the nonlocal d channel of our PP, by multiplying it by a factor –which we will call $1+\lambda$ –, thus deepening the d PP. As the nonlocal part of the PP vanishes outside the core radius, we are sure not to modify the Coulomb potential acting outside the core, and we preserve the shape of the PP as much as possible. As preliminary studies have shown that the d-bands depth depends exponentially on λ, we could chose a λ which has the desired effects on electronic structure, which we will discuss later on.

6.3.2 Effects on structure

As can be seen in Table 17, our modified PPs increases the PBE error on both lattice parameter and bulk modulus. The explanation for it is that a deepened d PP draws the d orbitals closer to the Zn nucleus, which thereby appears more screened for the Zn s orbitals, making those looser and more extended.

We also notice that ZnO is less affected than the other compounds, which likely originates from the interplay between the extension of s orbitals and the reduction of the p-d coupling, whose effect are opposite. As ZnO is more subject to p-d coupling than ZnS and ZnSe, the displacement of the d bands compensate a greater part of the effect on s orbitals.

6.3.3 Effects on electronic structure

We present here our data on the impact of various α and λ values (Table 18) on electronic properties of interest. First, a single choice of λ allows to have the d-bands less than 1 eV away from their experimental value in all compounds, an encouraging result. Secondly, our correction allows to recover the experimental gap for each compound with α varying within a range of 0.03, to be compared with the uncorrected case which require an alpha 0.10 bigger for ZnO than for other chalcogenides. Thirdly, the strong p-d mixing in ZnO

compound	λ	a Lattice	relative error	K [GPA]	relative error
ZnO	0	3.28	0.86%	128	-8.6%
	0.03	3.31	1.76%	125	-10.7%
	0.036	3.31	1.81%	124	-11.4%
	exp. [8,37]	3.25	/	140	/
ZnS	0	5.45	0.72%	69.2	-10.0%
	0.03	5.55	2.57%	63.1	-17.9%
	0.036	5.57	2.89%	62.3	-19.0%
	exp. [8,37]	5.41	/	76.9	/
ZnSe	0	5.74	1.17%	56.8	-9.8%
	0.3	5.83	2.90%	51.5	-18.3%
	0.36	5.85	3.21%	51.5	-18.3%
	exp. [8,37]	5.67	/	63	/

Table 17: Structural properties of ZnX compounds: experimental and PBE calculations with conventional and corrected pseudopotentials

is apparent again, in that the valence band maximum (VBM)–d-bands distance is less increased and the gap more widened than in ZnS and ZnSe, because the anion p bands are lowered more.

Parameters		ZnO		ZnS		ZnSe	
Alpha	Lambda	gap	d bands	gap	d bands	gap	d bands
0.000	0	0.77	5.01	1.97	6.15	1.06	6.27
0.000	0.03	1.7	7.02	2.41	8.41	1.5	8.79
0.000	0.036	1.83	7.68	2.48	9.1	1.57	9.51
0.250	0	2.69	5.33	3.64	6.78	2.78	7.14
0.250	0.030	3.74	7.41	4.10	9.19	3.23	9.68
0.250	0.036	3.87	8.05	4.17	9.88	3.31	10.39
0.347	0	3.49	5.64				
0.197	**0.036**	**3.42**	**7.98**				
0.192	**0.036**			**3.77**	**9.71**		
0.169	**0.036**					**2.74**	**10.11**
Exp. [8,37]		3.44	7.5-8.6	3.78	9.5	2.75	9.2

Table 18: Electronic properties of ZnX compounds: comparison of our corrected and uncorrected pseudo potentials with experiment; all energies in eV, d bands relative to the valence band maximum. **Bold**: our final estimate of the best choice of parameters for ZnO, ZnS and ZnSe respectively.

We should also underline that the increase in the gap width spawns from two effects: the reduced p-d coupling, and the weaker binding of Zn (s) orbitals, which form the conduction band minimum. The (un)physical origin of this effect will be discussed in detail on page 36.

The reduction of the p-d coupling using our modified pseudopotential has a threefold origin. In the estimation by eq. (18), $\epsilon_p^a - \epsilon_d^c$ is obviously increased, but also the bond length l_{bond} increases by 1-2%, and the radii of d orbitals r_d decrease, all factors leading to a weaker p-d coupling. The combination of these effects is so effective that, as an example,

d projected density of state in the p bands becomes small , even in ZnO (figure 16b). A contour plot of the lowest lying "p" band (figure 22) shows clearly how this band is in fact d dominated with a standard PP, while with our modified PP allows a true O (p) nature, with a small Zn (s, p) contribution.

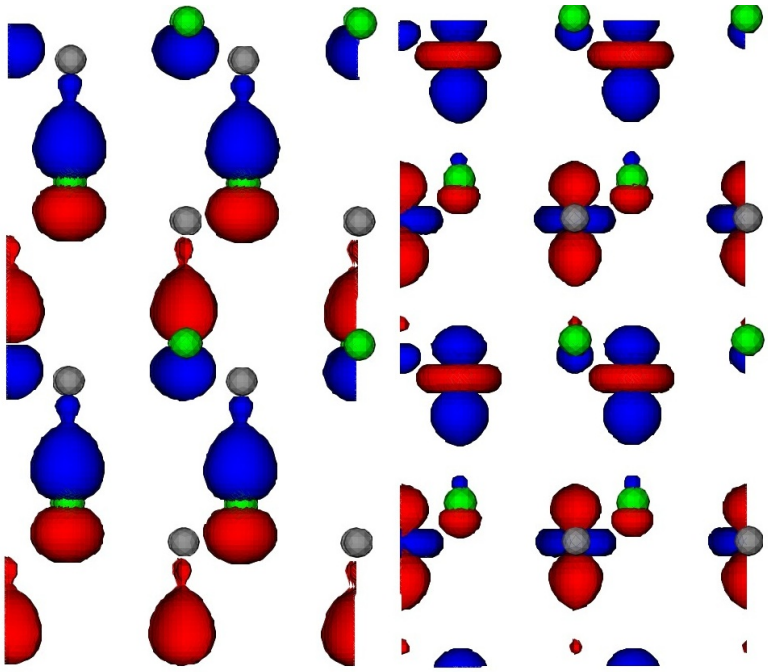

Figure 22: Lowest "p" orbital density of ZnO without (right) and with (left) pseudopotential modification, at the Γ point (red circled points in fig. 16) ; same isovalue plotted; grey atoms : Zn, green atoms: O; 8 repetitions of the unit cell are shown. Horizontal direction: [2100]; vertical direction: [0001].

Another visible effect of the reduced p-d coupling is the smaller width of the (d) band, as the energy difference between states of t_2 and e symmetry mostly comes from the p-d coupling, those states become much closer with our modification (Figures 16, 17 and 18).

Yet another observation is that the p bands become tighter, this again stems from two effects: the top of p bands is lowered due to reduced p-d mixing, and the bottom of it may get a bit higher because, among p states, it incorporates the most of Zn (s) character.

In the case of ZnO, we present a comparison of our calculations with experimental data on bulk bands (figure 23). We note in all cases that the p bands are not extended enough to fit the data from [64]; however with modified PP the dispersion is qualitatively better, especially at the bottom of p bands, were a band crossing occur between the first and second deepest p bands; the deepest p band has also a slope compatible with experiment going from M to Γ using our modified PP , even if it lies too high. We also notice that ref. [17] disagrees with ref. [39] on the positioning of d-bands, maybe because of a bad discrimination of bulk and surface states.

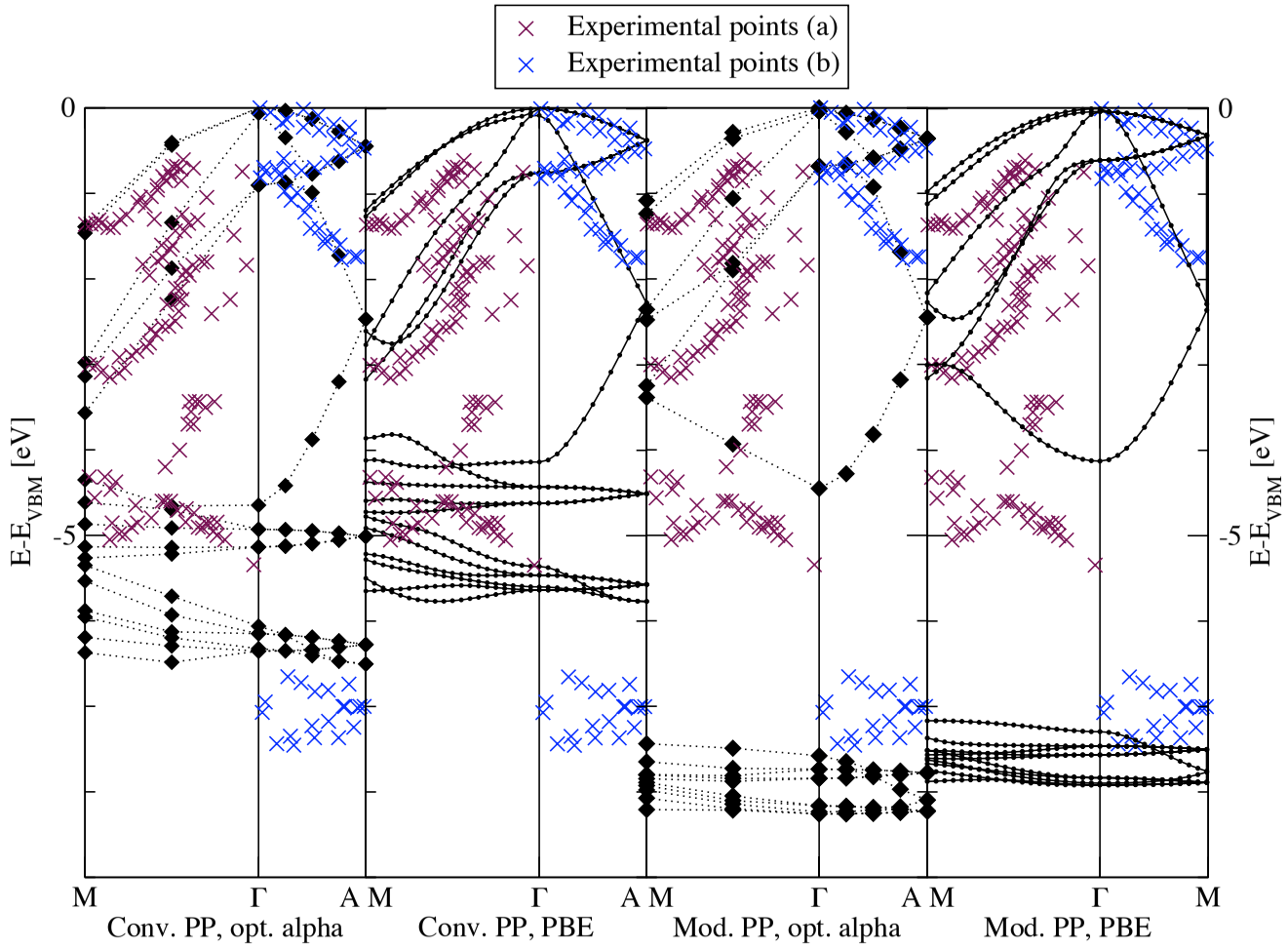

Figure 23: ZnO:Comparison of various calculations with experimental bands ; (a) : from [64], (b) : from [17]
.

6.3.4 Discussion

After listing the various effects of the PP modification on the studied systems, we discuss the relevance of this method on a more theoretical basis. a first question is whether the atomic d orbitals in the Zn atom are closer to our modified value than to the one obtained with a standard PP. However, experimental values for eigenvalues in isolated Zn atoms are hard to determine, thus we can only stick to the comment that our modification correspond better to the experimental values in bulk systems.
As was mentionned, d states are brought closer to the nucleus by our modification. Then, another question is whether this effect makes a better description of the "real" Zn atom, or if it is a spurious effect of the way we correct the energy of these states.

The effect on Zn (s) states needs be discussed as well: if d states are closer to the nucleus, s states will be less bound (by about 0.5 eV in our atomic PP calculations). This effect depends solely on the difference of the screening due to modified and non-modified d orbitals. It is not directly affected by how similar the non-modified (nor modified) d pseudo wavefunction is to the all-electron one. This is due to the fact that the non-modified pseudo s wavefunction will have the same eigenvalue as the all-electron one, independently from the shape of the d pseudo wavefunction from the PP generation.

However, a second aspect must be included in the present discussion : if we can assume that the ionic core is properly described in the PP, then the effect on s orbitals is the consequence of d being modified, no matter whether their modification is relevant or not. But here, we must refer to the theoretical section on unscreening (2.3.1)and to the section on Zinc pseudopotentials (4.2) : the ionic potential was "unscreened" using a certain valence density, which we think is modified in the modified PP, thus even though NLCC were not needed in the unmodified PP, they could be needed to ensure having only the direct effect of our modifications, and no spurious effects from the V_{XC} nonlinearity.

In summary, our PP modification supplemented by α adjustment has the following advantages:

- It allows correct placement of the d-bands without additional costs.
- It is less system dependant than a α-only modification.
- Bands are qualitatively better in ZnO.
- The overly d character of ZnO p bands is corrected.

On another hand, it shows the following inconvenient and/or open questions:

- It modifies the shape of d orbitals in a way whose physicality is not established,
- This has side effects on the Zn(s) orbital,
- This in turn affects structural properties in a undesirable way.
- Its justification at the atomic level is yet to assess.

7 Applications

Applications currently studied are ZnO doped with Co and ternary $ZnO_{1-x}S_x$. These applications are purposed to assess the usability of our method in more complex systems but are preliminary studies rather than *state of the art* calculations.

7.1 $ZnO_{1-x}S_x$

$ZnO_{1-x}S_x$ has been reported ([40]) to have hexagonal (*i.e.* wurtzite) structure, which is consistent with the fact that ZnS exists both as wurtzite and zincblende, while ZnO is only encountered as wurtzite. The electronic gap of ternary compounds such as $ZnO_{1-x}S_x$ in function of the composition is well described by the second order equation(22):

$$E_{ZnOS} = xE_{ZnS} + (1-x)E_{ZnO} + b(1-x)x \tag{22}$$

With $E_{compound}$ being the gap of a compound, x the concentration of sulphur, and b a "bending parameter" which depends on the constituents of the ternary alloy. In order to assess the applicability of our method in such a compounds, we will try to determine it's bending parameter.

Ternary compounds are likely to adopt a stochastic structure, whose proper description is a complex issue that we cannot address here. Instead we try to approach the dilute limits. Pure ZnO and ZnS wurtzite are simulated in a standard elementary cell approach. Mixed compounds are considered treated in a orthorhombic (*i.e.* $2a \times \sqrt{3}a \times 2c$) supercell of 32 atoms in the wurtzite structure, in which 1 of the 16 parent chalcogenide atom is replaced by the other element (*i.e.* $x = \frac{1}{16}, \frac{15}{16}$). The c/a ratio is kept from the parent compound, the a lattice constant is fixed as a linear interpolation between the two pure binary compounds, and the u parameter before relaxation is that the parent compound. The structure including the impurity atom is relaxed inside this fixed supercell at the PBE level. Hybrid calculations are run on those relaxed structure.For non-modified PP, no hybrid calculation was run, as the parent compounds do not share a common *ad-hoc* α, thus the choice of α would have been arbitrary. According to the consideration in sec. 6.3.4, we also include results for a modified PP based on a core-corrected PP.

Results and least-square fit can be found in figure 24. Ref. [40] reports an experimental bending parameter of approximately 3.0 eV. All our calculations overestimate this parameter ; the smaller error is found for the uncorrected PP using PBE functional, however unlike for other cases the regression fits the points only approximatively which leads to question the stability of this description. Furthermore, as the end points are not experimentally correct, this cannot be considered as a reliable description of those compounds.

The use of a core-corrected basis PP lead to a slightly better bending parameter. Overall, our methods do not allow to reproduce the experimental electronic gap bending parameter. One should note however that :

- Due to the form of Eq. (22), small errors in the dilute limits heavily impact the bending parameter.
- Similarly, the error on the gap of a compound is at most $\frac{1}{4}$ that on the bending parameter. (*i.e.* for $x = 0.5$, $x(1-x) = 0.25$)
- Experimentally produced $ZnO_{1-x}S_x$ may have non-uniform concentrations, random alloy structure, dislocations or interstitials which our simple structure does not reproduce.

Thus, these not too promising preliminary results should not be taken as overly conclusive, further work would be needed on that subject.

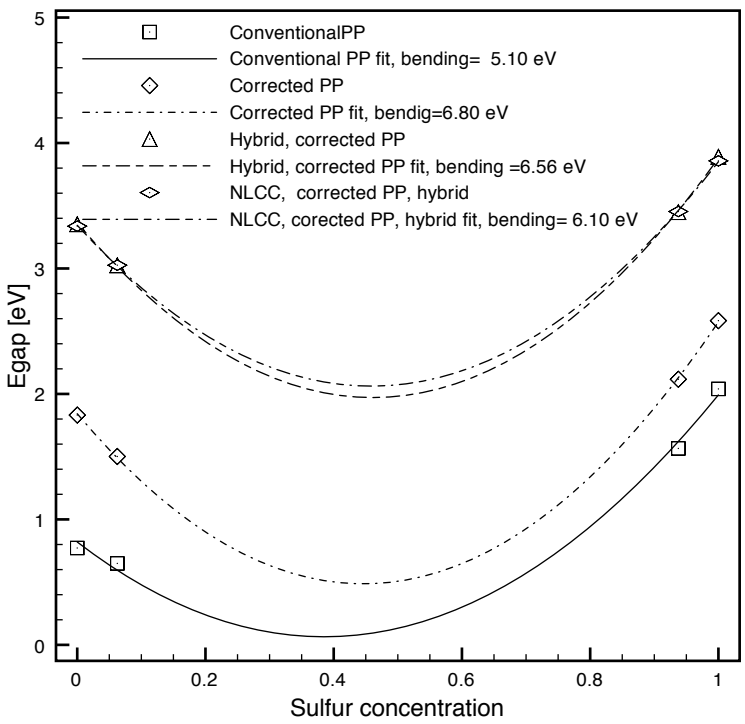

Figure 24: Gaps and bending parameters for ZnOS ternary compounds

7.2 Cobalt doped ZnO

To simulate cobalt doped ZnO, we used a hcp supercell made of $3 \times 3 \times 2$ elementary cells, *i.e.* 72 atoms. A Zn atom is replaced with a Co; starting from the ZnO structure for the considered PP, the atomic positions are relaxed at fixed supercell dimensions using only the gamma point of the Brillouin zone and the PBE XC functional. A $2 \times 2 \times 2$ k-points calculation in this relaxed configuration is considered the final result at the GGA level. Hybrid calculations were run as gamma only calculations; the hybrid calculation for a standard PP could not be converged due to oscillating magnetisation and limited execution time. Total and Co (d) up and down densities of states for finished calculations are shown in figures 25 26 and 27.

Ref. [28] experimentaly shows the cobalt minority spin states to be inside the band gap, with the e state 1.5 eV above valence band, and the t_2 state at the bottom of the conduction band. As was also reported in [62], the uncorrected GGA (Figure 25) calculation places the e states in the conduction band and the t_2 states even higher. Our corrected PP calculation shows the e state degenerated with the CBM, and the hybrid calculation using the corrected PP places the e state inside the gap, with however the t_2 state still lying in the conduction band. At this stage, two remarks need be made : first, the Co PP is not corrected in any way, even though it is a transition metal of the same row as Zn and thus likely subject to similar self-interaction problems. This could explain why Co (d) states lie too high in all our results. Secondly, as pointed out in ref. [62], the Co d-d splitting is more sensible to exact exchange than the ZnO gap, which means that an α sufficient to correct the ZnO gap will strongly overestimate the e-t_2 distance, making the hybrid approach unsuitable for this system. As both problem originate from

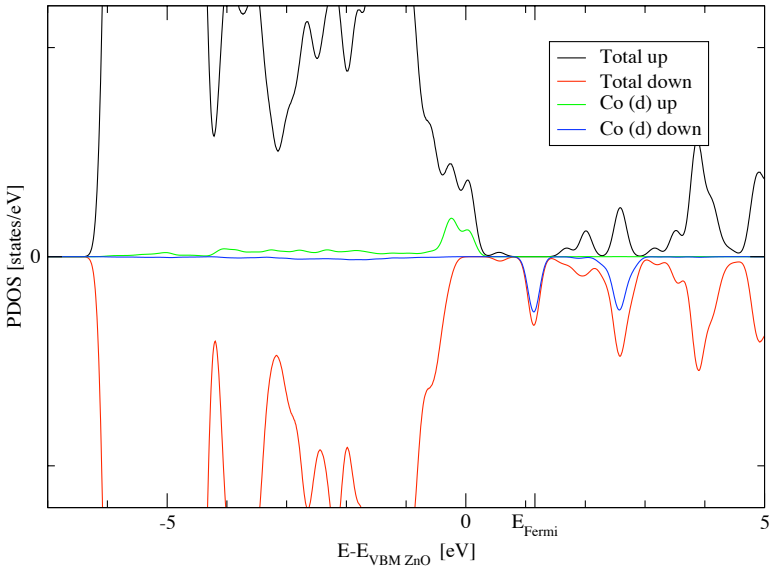

Figure 25: Projected densities of state for cobalt doped ZnO for a standard Zn PP using PBE XC functional

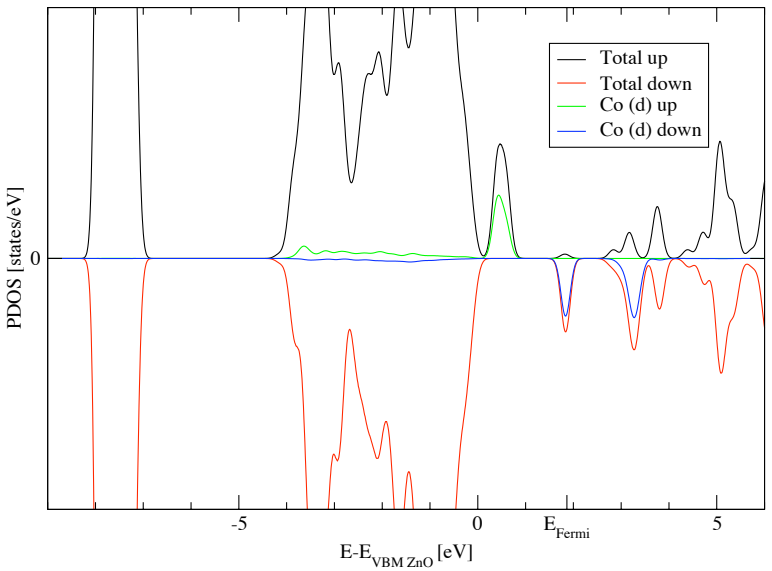

Figure 26: Projected densities of state for cobalt doped ZnO for a modified Zn PP using PBE XC functional

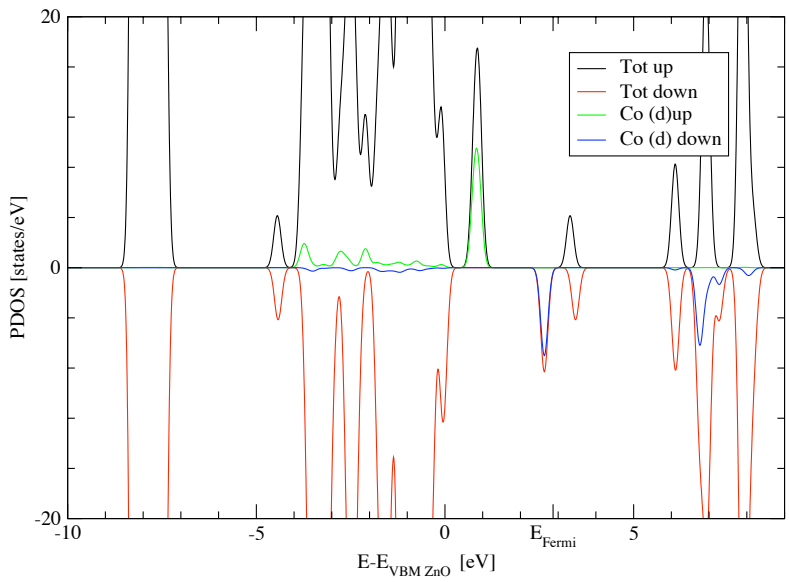

Figure 27: Projected densities of state for cobalt doped ZnO for a modified Zn PP using hybrid XC functional

the inclusion of another atom which requires proper treatment, this application doesn't allow to conclude on the suitability of our methods.

Further studies were run by Vladan Stevanovic, applying a similar *ad-hoc* PP modification to the Zn (s) channel in order to correct the gap without resorting on exact-exchange, and applying the same corrections to the Co PP, with the rationale that both elements belong to the same row of the periodic table. These PP were used in a orthorhombic $3a \times 2\sqrt{3}a \times 2c$ supercell (96 atoms) for a gamma-point PBE calculation. Preliminary results of this approach in figure 28; the s modification increase the d-VBM distance, which would require further adjustment of the d correction. This calculation yields approximately correct e and t_2 Co (d) states position. However, the s channel PP modification makes the lattice constant even more overestimated (by about 5 %), which is a notable drawback. This level of semi-empirical corrections is about the same as the one used in [62] for similar result, except they use DFA + U with Hubbard terms for Zn (d) and O (s). They do not mention any structural relaxation after the U parameter is added to the Hamiltonian, and therefore we cannot compare structural effects.

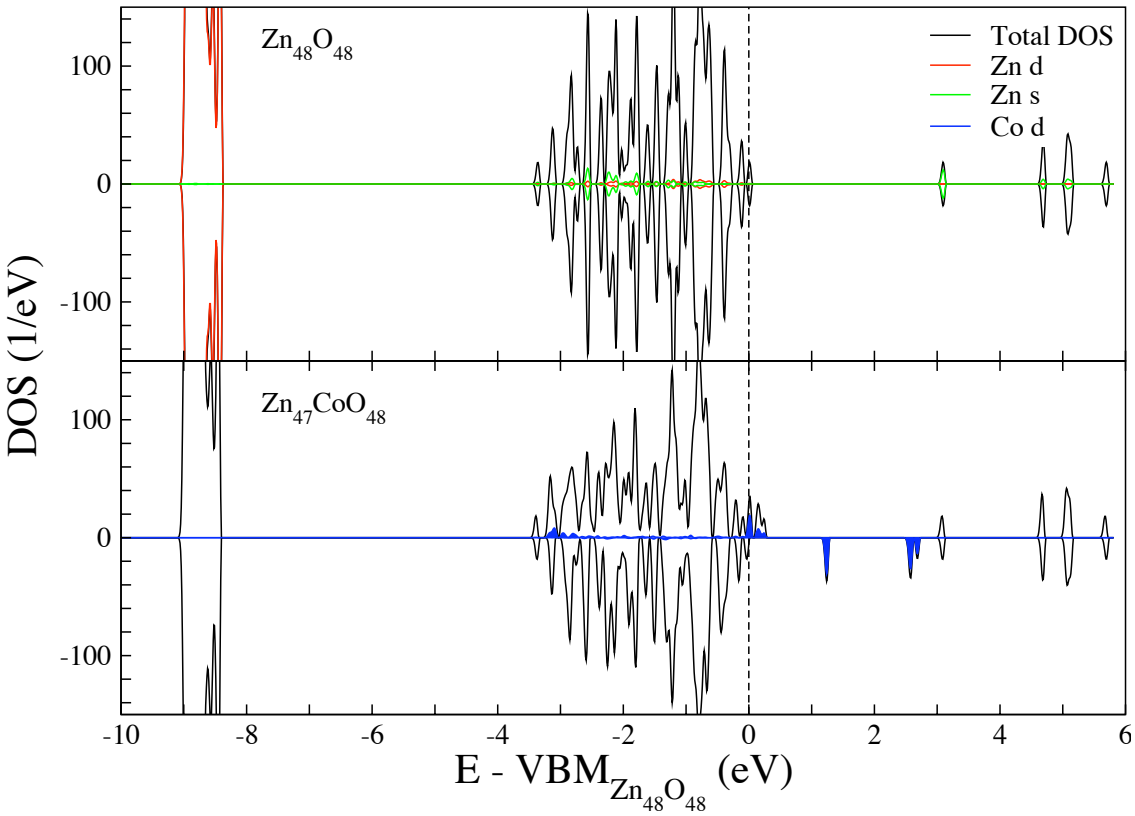

Figure 28: Projected densities of state for pure and cobalt doped ZnO using a d and s modified Zn PP and the PBE XC functional

8 Conclusion

In this work, we have studied the electronic and structural properties of II-VI compounds. A study of the relative stability of several phases of Mg-VI compounds was presented , as well as their electronic structure in the rocksalt phase using PBE and hybrid XC functionals.

We have also shown that d-bands positioning has crucial effect in zinc compounds, most prominently in ZnO, and thus description of these compounds needs a proper treatment of those states. We have shown that hybrid functionals on top of GGA-generated PPs are not an appropriate solution, and proposed a simple scheme to correct the GGA errors, allowing us to further highlight the Zn (d) orbitals role. The proposed scheme performs well in correcting the electronic structure of binary Zn-VI compounds, at some cost on structural properties. Up to now, applications of this scheme in more complex system have not proven successful, though they cannot be considered conclusive in a negative way either.

9 Acknowledgements

Thanks to :

Prof. A. Baldereschi, for allowing me to do this project.

Vladan Stevanovic, for supervision and advices.

Marc-Etienne Moret, for proof-reading and insightful discussions.

My family, for love, support and accommodation.

My Lord and Saviour Jesus-Christ, for a life worth living.

List of Figures

1 Illustration of rocksalt and zincblende structure 8
2 Illustration of the Brillouin zone for fcc systems 8
3 Illustration of the wurtzite structure 9
4 Illustration of the wurzite Brillouin zone 9
5 Core and valence densities in the zinc atom 13
6 All-electron and pseudo wavefunctions of zinc 13
7 Valence, core and pseudocore radial density for selenium 16
8 Valence, core and pseudocore radial density for cobalt 17
9 Energy vs volume plots for the three considered structure of the three magnesium compounds 19
10 PBE band diagrams and projected densities of states for MgO 21
11 PBE band diagrams and projected densities of states for MgS 21
12 PBE band diagrams and projected densities of states for MgSe 22
13 Dependence of MgO gap on the alpha parameter 22
14 PBE0 PDOS for MgO and MgS 23
15 *Ad-hoc* α (=0.316) PDOS for MgSe 24
16 Band diagrams and projected densities of states for ZnO 26
17 Band diagrams and projected densities of states for ZnS 27
18 Band diagrams and projected densities of states for ZnSe 28
19 Projected densities of states for ZnO using hybrid XC functionals 29
20 Projected densities of states for ZnS using hybrid XC functionals 29
21 Projected densities of states for ZnSe using hybrid XC functionals 30
22 Lowest "p" orbital of ZnO with and without modified pseudopotential . . . 34
23 ZnO:Comparison of various calculations with experimental bands 35
24 Gaps and bending parameters for ZnOS ternary compounds 38
25 Projected densities of state for cobalt doped ZnO for a standard Zn PP using PBE XC functional 39
26 Projected densities of state for cobalt doped ZnO for a modified Zn PP using PBE XC functional 39
27 Projected densities of state for cobalt doped ZnO for a modified Zn PP using hybrid XC functional 40
28 Projected densities of state for pure and cobalt doped ZnO using a d and s modified Zn PP and the PBE XC functional 41

List of Tables

1 Computed and experimental properties of magnesium metal 12
2 O_2 molecule 14
3 S_2 molecule 14
4 SO molecule 15
5 SeO molecule 15
6 SeS molecule 16
7 Calculations on bulk cobalt 17
8 Reported structures and band gaps of MgSe 18
9 Comparison of experimental data with our calculation for three MgSe structures 19
10 Comparison of PBE calculation with experiment for MgS and MgO rocksalt 20

11 Experimental and computed gaps for rocksalt Mg chalcogenides 20
12 PBE0 error on the gap and *ad-hoc* α parameter vs ionicity for rocksalt MgX 23
13 PBE0 results for zinc chalcogenides 25
14 Influence of the α parameter on electronic properties of zinc oxide 25
15 Estimation of the strength of *p*-*d* coupling in zinc compounds 30
16 Atomic eigenvalues for *d* and *p* orbitals of interest 31
17 Structural properties of ZnX compounds 33
18 Electronic properties of ZnX compounds 33

References

[1] Anisimov, V. I., Zaanen, J., and Andersen, O. K. Band theory and Mott insulators: Hubbard U instead of Stoner I. *Phys. Rev. B 44*, 3 (Jul 1991), 943–954.

[2] Ashcroft, N. W., and Mermin, N. D. *Physique des solides*. EDP Science, 2002.

[3] Becke, A. D. A new mixing of Hartree-Fock and local density-functional theories. *The Journal of Chemical Physics 98*, 2 (1993), 1372–1377.

[4] `http://www.abinit.org/Psps/?text=../Psps/GGA_FHI/fhi`

Pseudopotentials for the ABINIT code. World Wide Web electronic publication, 2008.

[5] `http:www.webelements.com`

Webelements: the periodic table on the web. Website. Collection of experimental data.

[6] Beltrán, A., Andrés, J., Calatayud, M., and Martins, J. B. L. Theoretical study of ZnO (1 0 *overline*1 0) and Cu/ZnO (1 0 $\bar{1}$ 0) surfaces. *Chemical Physics Letters 338*, 4-6 (2001), 224 – 230.

[7] Born, M., and Oppenheimer, R. Zur Quantentheorie der Molekeln. *Annalen der Physik,Volume 389, Issue 20 , Pages 457 - 484 389*, 20 (1927), 457–484.

[8] Broser, I., Broser, R., Finkelroth, H., Golazka, R., Grunlich, H., Hoffmann, A., Kossur, J., Mollwo, E., Nelkowski, H., Nimtz, G., Van der osten, W., Rosenzweig, M., H.J., S., Theis, D., and Tschink, D. *Semiconductors: Physics of II-VI and I-VII Compounds, Semimagnetic Semiconductors*. Springer-Verlag, 1982.

[9] Burke, K., Perdew, J., and Ernzerhof, M. Rationale for mixing exact exchange with density functional approximations. *J.Chem Phys. 105*, 22 (1996).

[10] Donnay, J. H., and Ondik, H., Eds. *Inorganic Compounds, Crystal Data, Vol. II*. Department of Commerce, Washington, DC, 1972.

[11] Drief, F., Tadjer, A., Mesri, D., and Aourag, H. First principles study of structural, electronic, elastic and optical properties of MgS, MgSe and MgTe. *Catalysis Today 89* (2004), 343–355.

[12] Engel, E., Höck, A., Schmid, R. N., Dreizler, R. M., and Chetty, N. Role of the core-valence interaction for pseudopotential calculations with exact exchange. *Phys. Rev. B 64*, 12 (Sep 2001), 125111.

[13] Feynman, R. Forces in molecules. *Phys. Rev. 56*, 340 (1939).

[14] Fu, C.-L., and Ho, K.-M. First principle calculation of the equilibrium ground state proprties of transitions metals: Applications to Nb and Mo. *Physical Rewiew B* (1983).

[15] Fu, J. Y., Liu, P. Y., Cheng, J., Bhalla, A. S., and Guo, R. Optical measurement of the converse piezoelectric d[sub 33] coefficients of bulk and microtubular zinc oxide crystals. *Applied Physics Letters 90*, 21 (2007), 212907.

[16] Fuchs, M., and Scheffler, M. Ab initio pseudopotentials for electronic structure calculations of poly-atomic systems using density-functional theory. *Comput. Phys. Commun.* (1998/99).

[17] Girard, R. T., Tjernberg, O., Chiaia, G., Söderholm, S., Karlsson, U. O., Wigren, C., Nylén, H., and Lindau, I. Electronic structure of ZnO(0001) studied by angle-resolved photoelectron spectroscopy. *Surface Science 373*, 2-3 (1997), 409 – 417.

[18] Gonze, X., Stumpf, R., and Scheffler, M. Analysis of separable potentials. *Phys. Rev. B 44*, 16 (Oct 1991), 8503–8513.

[19] Griebl, E., Haserer, B., Frey, T., Reisinger, T., and Gebhardt, W. $Zn_{1-x}Mg_xSe$ samples and a $ZnSe/Zn_{0.93}Mg_{0.07}$ Se quantum well under pressure: Optical absorption and photoluminescence. *Physica Status Solidi (b)* (1996).

[20] Gunshor, R., and Nurmikko, A. *II-VI Blue/Green light emitters : device physics and epitaxial growth*, vol. 44 of *SEMICONDUCTORS AND SEMIMETALS*. Academic press, San Diego, California, 1997.

[21] Hamann, D. R., Schlüter, M., and Chiang, C. Norm-Conserving Pseudopotentials. *Phys. Rev. Lett. 43*, 20 (Nov 1979), 1494–1497.

[22] Hellmann, H. *Einfuhrung in die Quantumchemie.* Franz Duetsche, Leipzig, 1937.

[23] Hohenberg, P., and Kohn, W. Inhomogeneous electron gas. *Phys. Rev. 136:B864-871* (1965).

[24] Hubbard, J. Electron correlations in narrow energy bands. *Proceedings of the Royal Society of London. Series A, Mathematical and Physical Sciences 276*, 1365 (1963), 238–257.

[25] Huber, K., and Herzberg, G. *Molecular spectra and molecular structure-IV Constants of diatomic molecules.* Van Nostrand Reinhold Company, 2004.

[26] Irikura, K. K. Experimental vibrational zero-point energies: Diatomic molecules. *Journal of Physical and Chemical Reference Data 36*, 2 (2007), 389–397.

[27] Jobst, B., Hommel, D., Lunz, U., Gerhard, T., and Landwehr, G. E_0 band-gap energy and lattice constant of ternary $Zn_{1-x}Mg_xSe$ as functions of composition. *Applied Physics Letters 69*, 1 (1996), 97–99.

[28] Kittilsted, K. R., Liu, W., and Gamelin, D. Electronic structure origins of polarity-dependent high-T_C ferromagnetism in oxide-diluted magnetic semiconductors. *Nature Materials 5* (2006), 291–297.

[29] Kleinman, L., and Bylander, D. M. Efficacious form for model pseudopotentials. *Phys. Rev. Lett. 48*, 20 (May 1982), 1425–1428.

[30] Kohn, W., and Sham, L. J. Self-consistent equations including exchange and correlation effects. *Phys. Rev., 140:A1133-1138* (1965).

[31] Lany, S., Raebiger, H., and Zunger, A. Magnetic interactions of Cr-Cr and Co-Co impurity pairs in ZnO within a band-gap corrected density functional approach. *Physical Review B (Condensed Matter and Materials Physics) 77*, 24 (2008), 241201.

[32] Lechi, H., Okawara, T., Sakai, M., and Nakanura, Masakazuand Kudo, K. Vertical-type organic device using thin-film ZnO transparent electrode. *Electrical Engineering in Japan 158*, 2 (2007).

[33] Litz, M. T., Watanabe, K., Korn, M., Ress, H., Lunz, U., Ossau, W., Waag, A., Landwehr, G., Walter, T., Neubauer, B., Gerthsen, D., and Schüssler, U. Epitaxy of $Zn_{1-x}Mg_xSe_yTe_{1-y}$ on (100)InAs. *J. Cryst. Growth 159*, 1-4 (1996), 54–57.

[34] Louie, S. G., Froyen, S., and Cohen, M. L. Nonlinear ionic pseudopotentials in spin-density-functional calculations. *Phys. Rev. B 26*, 4 (Aug 1982), 1738–1742.

[35] Löwdin, P.-O. On the non-orthogonality problem connected with the use of atomic wave functions in the theory of molecules and crystals. *The Journal of Chemical Physics 18*, 3 (1950), 365–375.

[36] Lunz, U., Schumacher, C., Nürnberger, J. N., Schüll, K., Gerhard, A., Schüssler, U., Jobst, B., Fsachingerand, W., and Landwehr, G. The energy gap E_g of $Zn_{1-x}Mg_xS_ySe_{1-y}$ epitaxial layers as a function of composition and temperature. *Semicond. Sci. Technol.*, 12 (1997), 970–973.

[37] Madelung, O., Rössler, U., and Van der osten, W. *Semiconductors: Intrinsic Properties of Group IV Elements and III-V,II-VI and I-VII Compouds.* Springer-Verlag, 1987.

[38] Martin, R. M. *Electronic Structure: Basic Theory and Practical Methods.* Cambridge University Press, 2004.

[39] Massidda, S., Resta, R., Posternak, M., and Baldereschi, A. Polarization and dynamical charge of ZnO within different one-particle schemes. *Phys. Rev. B 52*, 24 (Dec 1995), R16977–R16980.

[40] Meyer, B. K., Polity, A., Farangis, B., He, Y., Hasselkamp, D., Krämer, T., and Wang, C. Structural properties and bandgap bowing of

$ZnO_{1-x}S_x$ thin films deposited by reactive sputtering. *Applied Physics Letters 85*, 21 (2004), 4929–4931.

[41] Mittendorf, H. Röntgenographische und optische Untersuchungen aufgedampfter Schichten aus Erdalkalichalkogeniden. *Zeitschrift für Physik 183* (1965).

[42] Monkhorst, H. J., and Pack, J. D. Special points for Brillouin-zone integrations. *Phys. Rev. B 13*, 12 (Jun 1976), 5188–5192.

[43] Murnaghan, F. The compressibility of media under extreme pressures. *Proc. Nat. Acad. Sci. U.S.A. 10, 244* (1944).

[44] Okuyama, H., Nakano, K., Miyajima, T., and Akimoto, K. Epitaxial growth of ZnMgSSe on GaAs substrate by molecular beam epitaxy. *J. Cryst. Growth 117* (1992), 139–143.

[45] Patterson, C. H. Role of defects in ferromagnetism in $Zn_{1-x}Co_xO$: A hybrid density-functional study. *Physical Review B (Condensed Matter and Materials Physics) 74*, 14 (2006), 144432.

[46] Peiris, S. M., Campbell, A. J., and Heinz, D. L. Compression of MgS to 54 GPa. *The Journal of physics and chemistry of solids ISSN 0022-3697 55*, 5 (1994), 413–419.

[47] Pelucchi, E., Rubini, S., Bonanni, B., Franciosi, A., Zaoui, A., Peressi, M., Baldereschi, A., Salvador, D. D., Berti, M., Drigo, A., and Romanato, F. Structural and electronic properties of wide band gap $Zn_{1-x}Mg_xSe$ alloys. *Journal of Applied Physics 95*, 8 (2004), 4184–4192.

[48] Perdew, J. P., Burke, K., and Ernzerhof, M. Generalized Gradient Approximation made simple. *Phys. Rev. Lett. 77*, 18 (Oct 1996), 3865–3868.

[49] Perdew, J. P., and Zunger, A. Self-interaction correction to density-functional approximations for many-electron systems. *Phys. Rev. B 23*, 10 (May 1981), 5048–5079.

[50] Phillips, J. C. Ionicity of the chemical bond in crystals. *Rev. Mod. Phys. 42*, 3 (Jul 1970), 317–356.

[51] Puls, J., Rabe, M., Siarkos, A., and Henneberger, F. Excitonic properties of ZnSe/(Zn,Mg)Se quantum wells: A model study of the tensile-strain situation. *Phys. Rev. B 57*, 23 (Jun 1998), 14749–14757.

[52] Ramji Rao, R., and Ramanand, A. Thermal expansion and bulk modulus of cobalt. *Journal of Low Temperature Physics 26*, 3-4 (Februar 1977).

[53] Soldatov, A. V., Kravtsova, A. N., Fleet, M. E., and Liu, X. Unoccupied electronic states of MgS, CaS, FeS: x-ray absorption fine structure theoretical analysis. *Physica Scripta T115* (2005), 323–325.

[54] Stevanovic, V. Personnal discussion.

[55] Stifler, W. W. The magnetization of cobalt as a function of the temperature and the determination of its intrinsic magnetic field. *Phys. Rev. (Series I) 33*, 4 (Oct 1911), 268–294.

[56] Troullier, N., and Martins, J. L. Efficient pseudopotentials for plane-wave calculations. *Phys. Rev. B 43*, 3 (Jan 1991), 1993–2006.

[57] Ueda, K., Tabata, H., and Kawai, T. Magnetic and electric properties of transition-metal-doped zno films. *APPLIED PHYSICS LETTERS 79*, 7 (2001).

[58] Venkatesan, M., Fitzgerald, C. B., Lunney, J. G., and Coey, J. M. D. Anisotropic ferromagnetism in substituted zinc oxide. *Phys. Rev. Lett. 93*, 17 (Oct 2004), 177206.

[59] Verlet, L. Computer "experiments" on classical fluids. I. Thermodynamical properties of lennard-jones molecules. *Phys. Rev. 159*, 1 (Jul 1967), 98.

[60] Vogel, D., Krüger, P., and Pollmann, J. Ab initio electronic-structure calculations for II-VI semiconductors using self-interaction-corrected pseudopotentials. *Phys. Rev. B 52*, 20 (Nov 1995), R14316–R14319.

[61] Vogele, B., Morhain, C., Urbaszek, B., Telfer, S. A., Prior, K. A., and Cavenett, B. C. The influence of magnesium on p-type doping and opto-electronic properties of $Zn_{1-x}Mg_xSe$-based heterostructures. *Journal of Crystal Growth 201-202* (May 1999), 950–953.

[62] Walsh, A., Silva, J. L. F. D., and Wei, S.-H. Theoretical description of carrier mediated magnetism in cobalt doped ZnO. *Physical Review Letters 100*, 25 (2008), 256401.

[63] Wei, S.-H., and Zunger, A. Role of metal d states in II-VI semiconductors. *Phys. Rev. B 37*, 15 (May 1988), 8958–8981.

[64] Zwicker, G.and Jacobi, K. Experimental band structure of ZnO. *Solid State Communications 54*, 8 (May 1985), 701–704.